คอมพอสิตของอนุภาคแม่เหล็กระดับนาโนและเมโซพอรัสซิลิกาสำหรับการขจัดไอออนตะกั่ว (ll)

นายชวลิต ทาคูณ

วิทยานิพนธ์นี้เป็นส่วนหนึ่งของการศึกษาตามหลักสูตรปริญญาวิทยาศาสตรมหาบัณฑิต
สาขาวิชาปิโตรเคมีและวิทยาศาสตร์พอลิเมอร์
คณะวิทยาศาสตร์ จุฬาลงกรณ์มหาวิทยาลัย
ปีการศึกษา 2559
ลิขสิทธิ์ของจุฬาลงกรณ์มหาวิทยาลัย

MAGNETIC NANOPARTICLE-MESOPOROUS SILICA COMPOSITES FOR
LEAD(ll) ION REMOVAL

Mr. Chawalit Takoon

Thesis Title	MAGNETIC NANOPARTICLE-MESOPOROUS SILICA COMPOSITES FOR LEAD(ll) ION REMOVAL
By	Mr. Chawalit Takoon
Field of Study	Petrochemistry and Polymer Science
Thesis Advisor	Numpon Insin, Ph.D.
Thesis Co-Advisor	Wipark Anutrasakda, Ph.D.
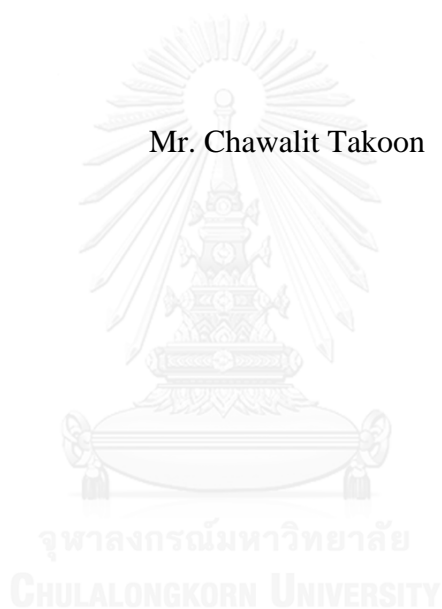
Accepted by the Faculty of Science, Chulalongkorn University in Partial Fulfillment of the Requirements for the Master's Degree

                                                          Dean of the Faculty of Science
        (Associate Professor Polkit Sangvanich, Ph.D.)

THESIS COMMITTEE

                                                          Chairman
        (Assistant Professor Warinthorn Chavasiri, Ph.D.)

                                                          Thesis Advisor
        (Numpon Insin, Ph.D.)

                                                          Thesis Co-Advisor
        (Wipark Anutrasakda, Ph.D.)

                                                          Examiner
        (Associate Professor Wimonrat Trakarnpruk, Ph.D.)

                                                          External Examiner
        (Tosapol Maluangnont, Ph.D.)

ชวลิต ทาคูณ : คอมพอสิตของอนุภาคแม่เหล็กระดับนาโนและเมโซพอรัสซิลิกาสำหรับการขจัดไอออนตะกั่ว (ll) (MAGNETIC NANOPARTICLE-MESOPOROUS SILICA COMPOSITES FOR LEAD(ll) ION REMOVAL) อ.ที่ปรึกษาวิทยานิพนธ์หลัก: ดร.นำพล อินสิน, อ.ที่ปรึกษาวิทยานิพนธ์ร่วม: ดร.วิภาค อนุตรศักดา, 65 หน้า.

คอมพอสิตแม่เหล็กระดับนาโนเมโซพอรัสซิลิกาชนิด MCM-48 (MNPs@MCM-48) ซึ่งถูกดัดแปรพื้นผิวด้วยลิแกนด์ที่มีหมู่ไทออล (-SH) และเอมีน (-NH$_2$) ถูกนำมาใช้ในการกำจัดไอออนตะกั่ว ตัวดูดซับที่สังเคราะห์ได้ถูกนำมาพิสูจน์เอกลักษณ์ด้วยเทคนิคฟูเรียร์ทรานสฟอร์มอินฟราเรดสเปกโทรสโกปี การเลี้ยวเบนของรังสีเอกซ์ กล้องจุลทรรศน์อิเล็กตรอนแบบส่องกราด กล้องจุลทรรศน์อิเล็กตรอนแบบส่องผ่าน การวิเคราะห์เทอร์โมกราวิเมทริกส์ และการวิเคราะห์พื้นที่ผิว ภาพถ่ายจากกล้องจุลทรรศน์อิเล็กตรอนแบบส่องกราดและผลการเลี้ยวเบนของรังสีเอกซ์แสดงให้เห็นว่าคอมพอสิต MNPs@MCM-48 มีขนาดอนุภาค 180 นาโนเมตร มีโครงสร้างแบบลูกบาศก์ มีพื้นที่ผิว 1,145 ตารางเมตรต่อกรัม และเมื่อถูกดัดแปรพื้นผิวด้วยไดเอทิลไตรเอมีนและ 2-อะมิโนไทโอฟีนอลจะเหลือ 863 และ 904 ตารางเมตรต่อกรัม ตามลำดับ ในการศึกษาการดูดซับตะกั่วด้วยเทคนิคเฟลมอะตอมมิคแอบซอร์พชัน พบว่าการดูดซับตะกั่วจะมีประสิทธิภาพที่ดีที่สุดเมื่อดูดซับตะกั่วที่ pH 5 และเวลาในการดูดซับ 2 ชั่วโมง โดยได้ค่าความจุการดูดซับสูงสุดที่ 202.13 และ 125.00 มิลลิกรัมต่อกรัมของตัวดูดซับที่ดัดแปรด้วยไดเอทิลไตรเอมีนและ 2-อะมิโนไทโอฟีนอลตามลำดับ วัสดุทั้งสองชนิดแสดงประสิทธิภาพการดูดซับไอออนตะกั่วถึงร้อยละ 100 ที่ความเข้มข้น 100 มิลลิกรัมต่อลิตร หรือต่ำกว่า ในภาวะดังกล่าว นอกจากนี้สารดูดซับทั้งสองชนิด ยังสามารถแยกออกจากน้ำหลังจากกระบวนดูดซับเสร็จสิ้นโดยการใช้แรงแม่เหล็กจากภายนอกอีกทั้งสารดูดซับทั้งสองยังสามารถกลับมาใช้ใหม่ได้ดีในการใช้ซ้ำครั้งที่ 2 ด้วยประสิทธิภาพของการดูดซับและความสามารถในการเก็บสารที่ถูกดูดซับที่เปลี่ยนแปลงเล็กน้อย

สาขาวิชา   ปิโตรเคมีและวิทยาศาสตร์พอลิเมอร์ ลายมือชื่อนิสิต _____

ปีการศึกษา 2559   ลายมือชื่อ อ.ที่ปรึกษาหลัก _____

                                         ลายมือชื่อ อ.ที่ปรึกษาร่วม _____

5572245123 : MAJOR PETROCHEMISTRY AND POLYMER SCIENCE

KEYWORDS: MCM-48 / MAGNETIC NANOPARTICLES / ADSORPTION / LEAD

> CHAWALIT TAKOON: MAGNETIC NANOPARTICLE-MESOPOROUS SILICA COMPOSITES FOR LEAD(ll) ION REMOVAL. ADVISOR: NUMPON INSIN, Ph.D., CO-ADVISOR: WIPARK ANUTRASAKDA, Ph.D., 65 pp.

Mesoporous materials-magnetic nanoparticles (MNPs@MCM-48)-based adsorbents containing thiol and amino groups were prepared and studied for Pb(II) ion removal. The obtained products were characterized by Fourier transform infrared spectroscopy, X-ray diffraction, scanning electron microscopy, transmission electron microscopy, thermogravimetric analysis and surface area analysis. SEM images and XRD patterns showed the particle sizes of around 180 nm and the cubic structure of MNPs@MCM-48, respectively. Surface areas of these adsorbents were determined to be ranging from 1,145 to 863 and 904 and m^2/g for the unmodified to diethylenetriamine and 2-amiothiophenol functionalized MNPs@MCM-48 samples. For the optimized sorbent formulation, the maximum adsorption capacities of 202.13 and 125.00 mg/g were observed at pH 5 and 2 h contact time as determined by flame atomic absorption spectroscopy. The removal efficiency was as high as 100% for Pb(II) at 100 mg/L and below. These sorbents were separated from water-based samples by an external magnetic field and can be reused limitedly, as the sorbents could be used for the second cycle with slight changes in the removal efficiency and adsorption capacity.

Field of Study:	Petrochemistry and Polymer Science	Student's Signature ....
		Advisor's Signature ....
Academic Year: 2016		Co-Advisor's Signature ....

ACKNOWLEDGEMENTS

CONTENTS

LIST OF TABLES

LIST OF FIGURES

LIST OF SCHEME

CHAPTER 1

INTRODUCTION

1.1 Statement of the problem

Lead is a toxic metal and a very strong poison. It is considered as a pollutant element worldwide. Humans can be easily exposed to lead via various pathways. If lead accumulates in the human body in high quantity, it can damage almost all vital systems in the human body including reproductive system [1] and nervous system [2]. For reproductive system, in men, not only the sperm count decrease when exposed to high concentration of lead, but lead can also change the sperm morphology and motility [3]. In a pregnant woman, lead can affect a child underdevelopment [4]. Children are the most sensitive to lead effects, and lead is absorbed at a faster rate compared to adults [5]. Lead is widely contaminated in dust and soil in lead mining, food, paints as well as waste water from petrochemical industry [6].

Different water treatment processes have been developed for removal and recovery of metal ions. The common treatment processes include chemical precipitation, coagulation and flocculation, ion exchange, electrochemical treatments, membrane filtration and adsorption technologies. Adsorption technologies are popular methods for the removal of heavy metals from industrial wastewater due to low cost, simple methods and high efficiency [7]. For materials to become an adsorbent for lead ions with best performance, the adsorbent must have pore structure and accessible adsorption sites. The adsorbent must be structurally stable under adsorption. Good contact should be established between the lead ions and the adsorption sites. Due to their characteristics of high surface area, large adsorption capacity and porous structure, MCM-48 and SBA-15 are regarded as good choices in wastewater treatments [8, 9]. However, MCM-48 and SBA-15 have a weak and low thermal stability bounding with metal ions. It is necessary to modify MCM-48 and SBA-15 to improve their thermal stability and adsorption capacity for metal adsorption application. For removal of metal ions in wastewater with nanoparticles of these materials to enhance the surface area, there are some problems because their particle sizes are so small that it is hard to collect them after the adsorption process. Functionalized Fe_3O_4 nanoparticles (NPs) were used as a support for removing sorbents from water by an external magnet [10].

MCM-48 cubic structures and SBA-15 hexagonal structures were chosen as sorbent materials in this work for their good adsorbent properties. Fe_3O_4 nanoparticles (NPs) were loaded into the adsorbents for superparamagnetic properties. The current work reports on the preparations of mesoporous silica and Fe_3O_4 nanoparticles. MCM-48 and SBA-15 were functionalized with thiol groups and amino groups for improving efficiency of adsorbents in lead in wastewater removal.

1.2 Objectives

1. Synthesis, functionalization and characterization of magnetic nanoparticle-mesoporous silica composites.

2. Investigation of selectivity, adsorption ability, and reusability of magnetic nanoparticle-mesoporous silica composites in lead (II) ion removal.

1.3 Scopes of the thesis

First, mesoporous silica (MCM-48 and SBA-15) were prepared via hydrothermal method, and Fe_3O_4 nanoparticles were synthesized by thermal decomposition method. Then Fe_3O_4 nanoparticles (NPs) were loaded into MCM-48 and SBA-15 to make magnetic composites. Fe_3O_4@MCM-48 and Fe_3O_4@SBA-15 were modified to improve the efficiency in removal of lead ion with diethylenetriamine (DETA) and 2-aminothiophenol (ATP). The formation of Fe_3O_4@MCM-48 and Fe_3O_4@SBA-15 was confirmed by X-ray diffractometer (XRD), Fourier- transform infrared spectroscopy (FT-IR), surface area analysis, thermogravimetric analysis (TGA). The morphology of Fe_3O_4@MCM-48 and Fe_3O_4@SBA-15 was studied using scanning electron microscopy (SEM) and transmission electron microscopy (TEM).

We present a study on the lead adsorption on amino- and thiol-functionalized Fe_3O_4@MCM-48 and Fe_3O_4@SBA-15 to compare the two functional groups that were functionalized on the potentially efficient supports. The adsorption of Pb(II) was studied by a batch operation. We studied effects of initial concentration of lead (II) ion, pH, and contact time in the removal of lead ion in water, including reusability of the sorbents. The concentration of lead solution was determined using flame atomic absorption spectrometry (FAAS).

CHAPTER 2
THEORY AND LITERATURE REVIEW

2.1 Mesoporous materials

Mesoporous materials are one of molecular sieve materials. From the IUPAC definition, porous solids are divided in 3 classes [11], and mesoporous materials are materials containing pores with diameters of between 2 and 50 nm, while microporous materials and macroporous materials have pores of diameter smaller than 2 nm and larger than 50 nm, respectively. Mesoporous materials have been used in many applications including ion exchange, drug delivery, catalysis and adsorption due to their large surface area, modifiable surface chemistry via functionalization, uniform pore size distribution and fast adsorption kinetics [12].
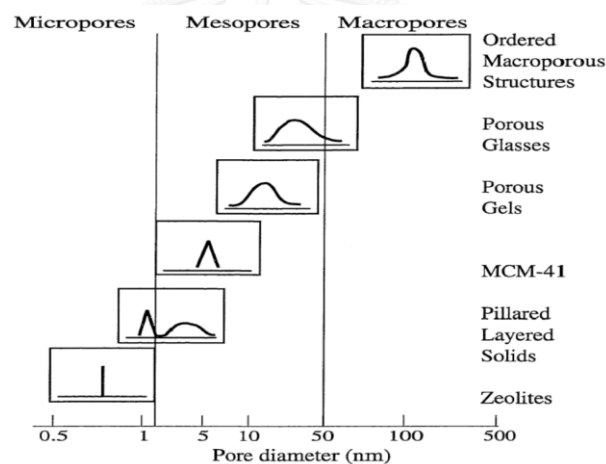
Figure 2.1 Definition and classification of porous Materials [11].

In 1992 mesoporous silica was first synthesized and prepared as highly ordered silica called M41S by Mobil scientists. The mesoporous materials M41S series have been classified into three main subgroups [13]: a hexagonal structure (MCM-41, SBA-15), a cubic structure (MCM-48), a lamellar structure (MCM-50). M41S and the SBA series are very popular in adsorption applications due to their structures and properties, but different from MCM-50 because MCM-50 materials have unstable lamella structure.
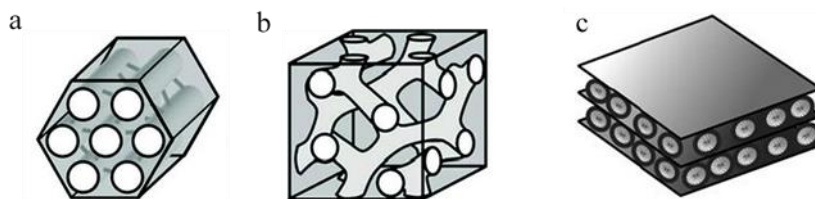
Figure 2.2 Structures of mesoporous M41S materials a) MCM-41 b) MCM-48 c)
MCM-50 [14].

2.1.1 Mobil Composition of Matter-48 (MCM-48）

Mobil Composition of Matter (MCM) was first synthesized by Mobil's researchers in 1992. MCM-48 has high surface area, a large pore volume, a strong thermal stability and three dimensional cubic pore structure. Due to MCM-48's 3-dimensional pore structure properties that could separate and eliminate diffusion limitations and prevent clogging, this material was more resistant to pore blocking and could achieve faster diffusion with good mass transfer through the channels [15]. Surfaces of MCM-48 structure can be modified, and loading transition metals into its framework can be done to apply this materials in catalytic and adsorption applications.

2.1.2 Santa Barbara Amorphous-15 (SBA-15）

Santa Barbara Amorphous was developed in 1998 by Zhao *et al.*[16] SBA-15 is a mesoporous silica with a narrow pore size distribution and a tunable pore diameter of between 5 and 30 nm. It can make the target molecules come into material pores with less difficulty. SBA-15 has two-dimensional hexagonal pore structure. The thickness of framework walls of SBA-15 are about 4 nm, which gives the material a higher mechanical and hydrothermal stability than MCM-41 （thickness of MCM-41 wall is about 1 nm） [17].

2.1.3 Principles of the synthesis of mesoporous materials

Four reagents were required to synthesize mesoporous materials.

1. Solvent

Water or alcohol was used for synthesis of mesoporous silica.

2. Silica sources

Tetramethyl ortosolicate (TMOS), tetraethyl ortosilicate (TEOS), and sodium silicate were used as inorganic species of silica.

3. Catalysts

Acids and bases were used for bringing the reaction mixture to acidic or basic conditions, respectively. Moreover, they act as catalysts for the hydrolysis and condensation of silica precursors.

4. Surfactants

Surfactants are molecules that have a dual chemical property in the structure; one part of the molecule is hydrophilic and the other is hydrophobic [18].

Surfactant can be classified into 4 groups according to the charges of the head group.

Anionics (S⁻): A type of surfactants that have negative charges on polar head groups such as carboxylates, sulphates, sulfonates and phosphates.

Cationics (S⁺): A type of surfactants that have positive charges on polar head group. Most used cationic surfactants are fatty amines, their salts, and quaternary derivatives. Cationics surfactants are mostly based on nitrogen atom.

Non ions (S^0) : A type of surfactants that do not produce ions in aqueous solution. Examples are poly(ethylene oxide) and block copolymers. The copolymers are composed of blocks of different polymerized monomers, and they usually have a relatively low molar mass.

Zwitterionics : A type of surfactants that have two different charges of different signs on their head group giving a neutral charge. In other words, they have both cationic and anionic centers attached to the same molecule. Ammonium cations are most common for positively charged group, and carboxylate are most common for negative charged group, but the composition may vary using other groups such as sulfonates group.
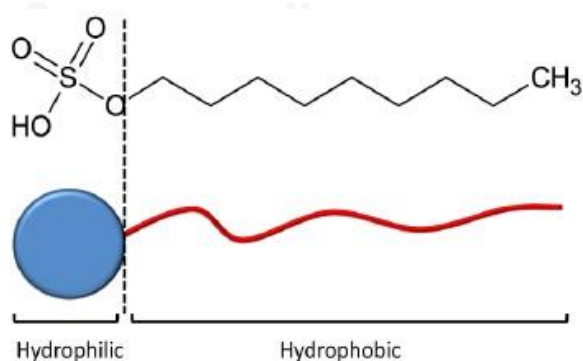
Figure 2.3 Basic diagram of surfactant structure [19].

The structures of resulted mesoporous materials depend on the electrostatic and steric interaction between silica sources and the surfactant molecules. The charging of surfactants (S) are determined by their property, while the charging of silica sources (I) are determined by pH of the synthesis system. For the interaction between surfactants and silica sources with different charges can be completed by the reverse charge matching (S^-I^+ or S^+I^-). Also, the interaction between similar charges could be done under the mediation of ions with the opposite charge ($S^+ X^- I^+$ or $S^- X^+ I^-$). However, anionic surfactants as the template are not suitable for the synthesis of mesoporous materials because in basic condition the interaction of surfactant and silicate are very weak, and under acidic condition anionic surfactant could receive the large number of protons from acid solution. For non-ionic surfactant, the surfactant was interacted with silica sources through hydrogen-bonding for controlling the structure of mesoporous materials (S^0I^0) , ($S^0(IX)^0$) [19].
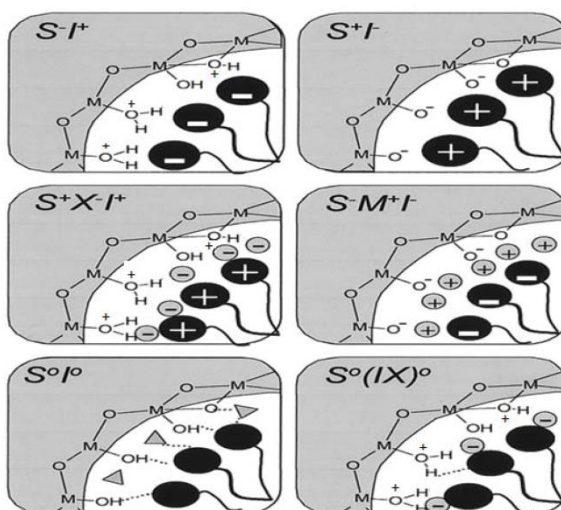
Figure 2.4 Different types of silica-surfactant interactions [19].

Formation mechanism of mesoporous materials was divided into 2 pathways.

1. The liquid crystal templating mechanism [20].

The surfactant liquid crystalline phase was formed before the hydrolyzed silica sources with hydrophilic character were filled into liquid crystalline phase. The geometry of mesoporous materials depends on the liquid crystalline shape.

2. Cooperative formation mechanism [21].

The silica source was added into the mixture to form the template of mesopores via the self-assembly process.
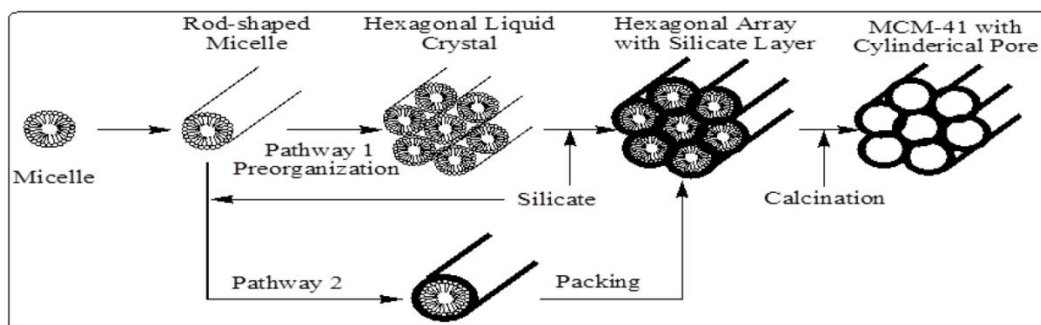
Figure 2.5 Schematic model of microporous formation mechanism via two possible pathways a) The liquid crystal templating mechanism and b) Cooperative formation mechanism [20].

The shape and the aggregation of micelles into liquid crystals depends on the surfactant concentration [22]. At very low concentration, surfactants dissolve in solution and act as free molecules. When surfactant concentration is higher and reach the CMC1 point (critical micelle concentration 1), the surfactants are formed into small spherical micelles, and at the CMC2 point (critical micelle concentration 2) for higher surfactant concentration, small spherical micelles coalesce to form cylindrical micelles as the quantity of solvent between the micelles are decreased. When the surfactants concentration is higher than the CMC2 point and the liquid crystal (LC) are aggregated to form hexagonal close-packed LC arrays. Moreover, cubic structure are formed when the surfactant concentration is higher than concentration for the formation of hexagonal[22].
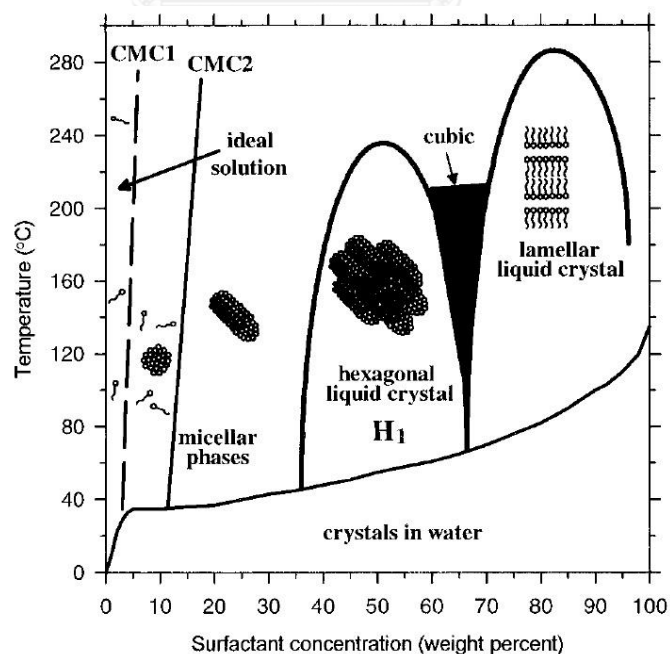
Figure 2.6 Phase diagram of a quaternary ammonium surfactant (cetyltrimethylammonium bromide: CTAB) in water [22].

The solutions are mixed and aged at appropriate temperature and time. After crystallization, the surfactant template is no longer needed, and it is removed to open the porous structure by calcination, solvent extraction or UV-ozone treatment.

2.1.4   Removal of the surfactant template

The removal of surfactant is the important step for synthesis of mesoporous silica as the surfactant molecules used as templates must be removed to yield the porous structures. Various methods, such as calcination, solvent extraction and UV-Ozone treatment are common methods for removing surfactant templates from mesoporous silica.

1.Calcination

Calcination is a common method used for removal of the template in materials. The as-synthesized materials are composed of huge amounts of coke and organic impurities, and these contaminants can block the pore in the materials. Therefore, this method is also used to solve a pore blocking problem. For this method, the as-synthesized materials are heated in air, nitrogen and oxygen. When the template is removed from mesoporous materials, the mesoscopic structure is well organized, and the reflection intensities are usually increased. A standard common procedure that can be used in the calcination of mesoporous silica is a temperature program of a heating rate of 1 °C/min up to 550°C under air for 5 h [23] .

2.Solvent extraction

Solvent extraction is based on the extraction of the organic templates.   The efficiency of solvent extraction depends on the interactions between the templates and the inorganics, temperature and extraction time. MCM-41 and MCM-48 can be extracted in alcohols, acid solutions, ammonium acetate and neutral salt solutions, etc. Block copolymers can be extracted from SBA-15 with acidic ethanol solutions [24]. More polar solvents, such as strong acid, are good choices to dissolve the template ions. Ion-exchange is the reaction during the removal of templates using solvent extraction.

3.UV-Ozone

In this method, the as-synthesized mesoporous silica is treated with ozone using a UV lamp with specific wavelength to produce ozone from atmospheric oxygen. The non-ionic surfactants are then removed from mesoporous silica structure at room temperature [25].

Calcination is the most popular method to remove the surfactant template because calcination is a facile process and could eliminate the surfactant templates used in the materials with high temperature. However, this method requires a large quantity of energy to remove surfactant template, and the mesoporous structures of the materials could be broken after calcined at high temperature for a long of time [26]. Solvent extraction is used to avoid the destructive effect, but this method need a large amount of organic solvents and a long time requirements. Solvent extraction can efficiently

extract the templates from mesoporous materials at temperatures between 50 and 100 °C. For UV-Ozone treatment, the templates can efficiently be extracted from mesoporous materials at temperatures not exceeding 250 °C. The advantages of ozone treatment are that this method does not require organic solvents to remove the templates on materials, and the resulted samples yield a high silanol group density. However, toxic gases can form and pollute the atmosphere after removal of the surfactant templates, and this method cost highly when compared with calcination and solvent extraction methods [27].

2.2. Iron oxides and their magnetic properties

Iron oxides are chemical compounds composed of iron and oxygen. Iron oxides include magnetite, hematite and maghemite. Hematite shows an antiferromagnetic property, while magnetite and maghemite shows a ferrimagnetic property [28].

Generally, the magnetic materials are divided into three classes by their properties [29].

1. Diamagnetic is the weakest magnetic properties with negative susceptibility to a magnetic field. In these materials, a small magnetization is induced when placed near strong magnets and does not maintain the magnetic properties when the external field is removed [30].

2. Paramagnetic is the stronger magnetic property than diamagnetic with positive susceptibility to magnetic fields. Paramagnetic properties are due to the presence of some unpaired electrons. Magnetic moments are arranged into the same direction when placed under an external magnetic field. In other words, magnetic moments of the paramagnetic material have random directions when placed outside a magnetic field[30].

3. Ferromagnetic is the strongest magnetic properties with positive susceptibility to an external magnetic field. These materials show permanent magnetization, and ferromagnetic materials show a strong attraction to magnetic fields. Moreover, the materials are able to retain their magnetization after the external field has been removed [29]. Ferromagnetism consists of two subclasses, ferrimagnetism and antiferromagnetism. For ferrimagnetism, the materials would attractively respond to an external magnetic field, but with more weakly than ferromagnetic materials of the same quantity. For antiferromagnetism, the materials show very little magnetization when placed under magnet fields.

For nanomaterials, superparamagnetic is a type of magnetic character that exhibits in ferromagnetic and ferrimagnetic nanoscales. The nanoparticles are single-domain particles. In other words, total magnetic moment of the nanoparticle can be considered as one giant magnetic moment. The materials conduct similar to paramagnetic materials in absence of magnetic fields, but superparamagnetic materials have much stronger magnetic response than paramagnetic materials [30].

2.2.1 Magnetite

Magnetite is a ferrimagnetic material with crystal structure following an inverse spinel structure with octahedral and tetrahedral-octahedral layers. The chemical formula Y[XY]O$_4$ with X and Y symbolize ferrous and ferric, respectively. In magnetite structure, ferrous ions inhabit the octahedral lattice sites, and ferric species stay in the other octahedral and tetrahedral lattice sites. Magnetite's density is confirmed at 5.18 g/cm^3 and melting/boiling points are noted at 1590 and 2623 °C. Magnetite has a face-centered cubic lattice structure with a unit cell edge length of 0.8396 nm and exhibits twinning along {111} planes [31].
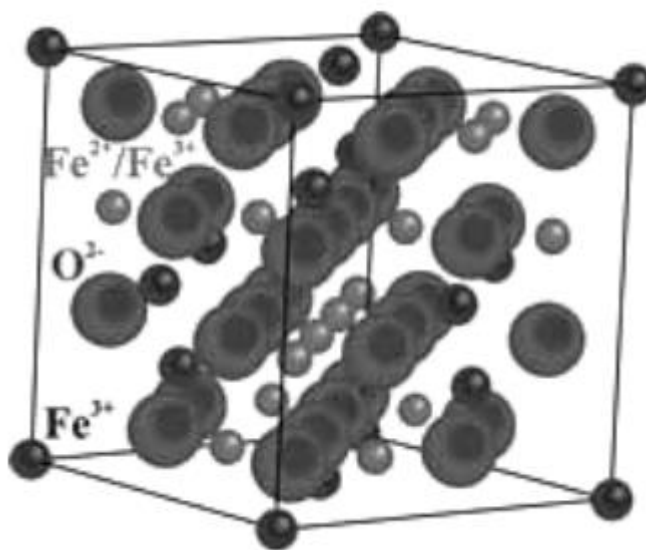
Figure 2.7 A unit cell of magnetite [31].

For this work, magnetite particles in nanoscale were used to form composites with mesoporous silica for their high magnetization and relatively low toxicity. The resulted composites were proposed to be sorbents that could be magnetically separated from treated water.

2.3 Adsorption

Adsorption is a process of gas, liquid or solid phase transferred from one substance into another substance surface via mass transfer. A substance to be adsorbed on a surface are called adsorbate. The surface solid that adsorbs another substance is called adsorbent. This is a different process from absorption as adsorption happens at the surface of the substance but absorption is a term describing the distribution of the substance entering some bulk phase material. If adsorption and absorption are happening at the same time, the process is called sorption.

2.3.1 Physical adsorption

The physical adsorption occurs with the structure of multilayer of adsorbate on adsorbent. The force of attraction between adsorbate and adsorbent is weak van der Waal forces of attraction. The process is reversible, and the physical adsorption decreases with increase of temperature. This type of adsorption has low enthalpy of adsorption of about 20-40 kJ/mol.

2.3.2 Chemical adsorption

The chemical adsorption takes place with the structure of monolayer of adsorbate on adsorbent. The force of attraction between adsorbate and adsorbent is chemical forces or chemical bonds. The process is irreversible, and the chemical adsorption first increases and then decreases with increase of temperature. The effect is called activated adsorption. This type of adsorption has high enthalpy of adsorption of about 40-400 kJ/mol.

Coordination and the Hard/Soft Acid/Base (HSAB) theory

Coordination bonds could be formed between a metal center and ligands (atoms, ions, or molecules that donate electrons to the metal). These coordination compounds or complexes can be neutral or charged. The formation of these compounds can be explained using the hard/soft acid/base theory. Hard acids and bases are small, compact, and non-polarizable species, while soft acids and bases are larger molecules or ions with more diffused distribution of electrons. Borderline acids are intermediate between hard and soft acids as they have lower charge and larger size than hard acids, and higher charge and smaller size than soft acids. Borderline bases are intermediate between hard and soft bases similar to the borderline acids[32].

The polarizability of an acid or base plays an important role in its reactivity. Hard acids (ions of hard metal) form more stable complexes with hard bases (hard ligands), while soft acids (ions of soft metal) shows a preference for soft bases (soft ligands). Borderline acids and bases showed less preference on the pairing with the counterparts, leading to difficulty in finding the stable complexes for these species. Lead (II) ion is regarded as a borderline acid [33], and therefore challenging in finding the bases that could form stable complexes.

2.3.3 Adsorption isotherm

The process of adsorption is studied through graphs about the quantities of adsorbate adsorbed on the surface of adsorbent at a constant temperature. Langmuir, Freundlich and BET model are common isotherms for removal of metal ions in waste water treatment [34].

The Langmuir isotherm [35]

The Langmuir isotherm studies adsorption of adsorbate via monolayer adsorption onto the homogenous surface of adsorbent at a constant temperature. The surface of adsorbent has a specific number of sites where adsorbate molecules can be adsorbed. The Langmuir isotherm is shown in Eq. 2.1.

$$q_e = \frac{Q_0 b C_e}{1 + C_e b};$$ (2.1)

where

q_e = the amount of metal adsorbed per gram of the adsorbent at equilibrium (mg/g);
C_e = the equilibrium concentration of adsorbate (mg/L);
Q_o = maximum monolayer coverage capacity (mg/g);
b = Langmuir isotherm constant (L/mg).

The linear form of the Langmuir equation is shown as Eq. 2.2. [38]

$$\frac{C_e}{q_e} = \frac{1}{Q_0 b} + \frac{1}{Q_0} C_e$$ (2.2)

The Freundlich isotherm [36]

The Freundlich isotherm studies adsorption of adsorbate via multilayer adsorption onto the heterogeneous surface of adsorbent at a constant temperature. The Freundlich isotherm is shown in Eq. 2.3.

$$q_e = K f C_e^{1/n};$$ (2.3)

where
K_f = Freundlich isotherm constant (mg/g);
n = adsorption intensity;
C_e = the equilibrium concentration of adsorbate (mg/L);
q_e = the amount of metal adsorbed per gram of the adsorbent at equilibrium (mg/g).

The linear form of the Freundlich equation is written as Eq. 2.4.

$$\ln q_e = \left(\frac{1}{n}\right) \ln C_e + \log k$$ (2.4)

where
n = adsorption intensity;
q_e = the amount of metal adsorbed per gram of the adsorbent at equilibrium (mg/g);
K_f and $1/n$ can be determined from the linear plots of $\ln q_e$ versus $\ln c_e$.[39]

2.4 Literature reviews

Mesoporous silica materials have been widely used in adsorption applications for removal of lead due to their properties of large surface area, narrow distribution pore size and good kinetics. However, mesoporous silica materials are not efficient for direct lead adsorption. Mesoporous silicas have to be modified with various functional groups for improving adsorption efficiency. In many researches, different functional groups were used to functionalized with mesoporous silica and magnetic-mesoporous silica in the removal of lead in waste water as summarized in Table 2.1.

Table 2.1 Functionalized mesoporous silica for removal of lead ions

Adsorbent	Ligands	Adsorption capacity (mg/g)	References
MCM-41	$CH_3(CH_2)_{10}CH_2\overset{\underset{CH_3}{\vert}}{N}CH_3$	84.95	[8]
MCM-41	$CH_3(CH_2)_{10}CH_2NH_2$	51.8	[8]
SBA-15	$H_3CO-\overset{\underset{OCH_3}{\vert}}{\overset{\overset{OCH_3}{\vert}}{Si}}\sim NH_2$	82.88	[37]
SBA-15	$HS\sim\overset{\underset{OCH_3}{\vert}}{\overset{\overset{OCH_3}{\vert}}{Si}}-OCH_3$	39.36	[38]
MCM-41	$H_3CO-\overset{\underset{OCH_3}{\vert}}{\overset{\overset{OCH_3}{\vert}}{Si}}\sim NH_2$	35.22	[39]
MCM-41	$HS\sim\overset{\underset{OCH_3}{\vert}}{\overset{\overset{OCH_3}{\vert}}{Si}}-OCH_3$	87.02	[39]
MCM-41	$H_2N\sim\overset{\underset{H}{\vert}}{N}\sim NH_2$	192.69	[39]
Mag-MCM-41	$H_3CO-\overset{\underset{OCH_3}{\vert}}{\overset{\overset{OCH_3}{\vert}}{Si}}\sim NH_2$	268	[40]
Mag-MCM-48	triazine with three NH₂ groups	127.24	[41]
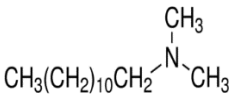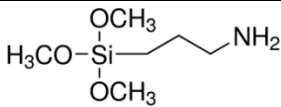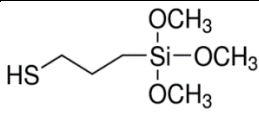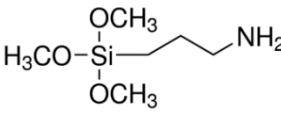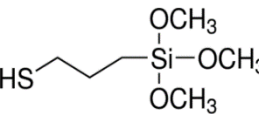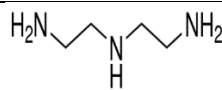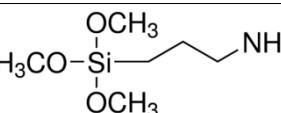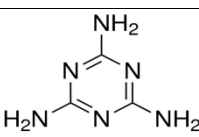
For Benhamou, A. *et al*. [8], mesoporous silica MCM-41 was synthesized using 1 SiO_2, 0.45 CTAB, 0.32 TMAOH, $67H_2O$. Surface area of calcined MCM-41 was 1207 m^2/g, and the pore volume was 0.853 cm^3/g. The functionalized MCM-41 with N-N dimethyldodecylamine (DMDDA) and dodecylamine (DDA), N-N dimethyldodecylamine (DMDDA) and dodecylamine (DDA) were added into MCM-41 each batch under magnetic stirrer at ambient conditions. Surface area of DMDDA-MCM-41 and DDA-MCM-41 were 63 m^2/g and 89 m^2/g and pore volume 0.276 cm^3/g and 0.314 cm^3/g, respectively. Each sample exhibited type IV isotherm according to the IUPAC classification with hysteresis loops. For lead adsorption in mixed solution experiment, the adsorption capacity of lead (II) ion using DMDDA-MCM-41 and DDA-MCM-41 were 84.95 mg/g and 51.8 mg/g, respectively.

For Yang, H. *et al.* [37], SBA-15 with cetyltrimethylammonium (CTAB) and tetramethyl ammonium hydroxide (TMAOH) as hybrid surfactant templates was synthesized with APTES, TEOS, CTAB, HCl, TMAOH, ethanol molar ratios of 0.25:1:0.022:0.025:6.25:40.76 in a one- step procedure. In other words, the functionalization directly incorporated organic groups into silica frame. After that, the solvent extraction was used to remove organic template. Surface area of 421.9 m^2/g , pore volume of 0.556 cm^3/g and pore size of 6.1 nm were reported for APTES-SBA-15. The nitrogen adsorption–desorption isotherm showed the Type-IV curve. The ability of adsorbent to remove lead ions from aqueous solution showed that the adsorption capacity was 82.88 mg/g.

For Thuu, P. *et al.* [38], thiol-functionalized-SBA-15 materials were synthesized by varying the concentration of 3-mercaptopropyltrimethoxysilane (MPTMS) as a thiol source with different molar ratios of MPTMS/TEOS of 0.05, 0.10, 0.15, 0.20, and 0.30. This method used ligand functionalization with a one-step procedure. The surface area SBA-15 with 0.05 MPTMS/TEOS molar ratios was 720.7 m^2/g, pore size was 6.1 nm, and the surface area and pore size were decreased with increase of thiol group. All samples are type IV adsorption isotherms. The results of lead adsorption depended on amount of thiol group in the functionalized SBA-15 samples while the adsorption capacity of thiol-functionalized mesoporous silica with 0.30 MPTMS/TEOS molar ratios was 39.36 mg/g.

For Idris, S. *et al.* [39], different groups of APTES MPTMS and DETA were used as agents for amino and mercapto functional groups for surface modification onto MCM-41. The synthesis process of MCM-41 was modified to improve silanol group and pore distribution. Solution of nitric acid and hydrogen peroxide were used in microwave digestion (MWD) to remove the surfactant. The surface and pore size of MWD-MCM-41 and C-MCM-41(calcination method) were 760 m^2/g , 6.74 nm and 813 m^2/g, 2.53 nm , respectively, while MWD-MCM-41 has larger pore size than C-MCM-41. The adsorption isotherm MWD-MCM-41 showed Type IV with the hysteresis loop. MWD-MCM-41 loop was broader than C-MCM-41 loop that show MWD-MCM-41 have a large pore distribution with the different pore size. MWD-MCM-41 was brought to use as materials for functionalization with ligands to improve adsorption efficiency using a condensation reaction. The adsorption capacity of

APTES-MCM-41, MPTMS-MCM-41 and DETA-MCM-41 were 35.22 mg/g, 87.02 mg/g and 192.69 mg/g, respectively.

For Mehdinia, A. *et al.* [40], magnetic mesoporous silica nanocomposites were synthesized using colloidal suspension of magnetic nanoparticles under nitrogen atmosphere. The surfactant templates of mesoporous silica composite were removed by calcination, and APTES was added into mesoporous silica composites for surface modification. The adsorption isotherm of magnetic mesoporous silica nanocomposites showed type IV of mesoporous structure. The surface area magnetic mesoporous silica nanocomposites was 880 m^2/g, and the pore size was 1.8 nm. The magnetic amine-functionalized mesoporous silica nanocomposites were used to remove lead(II), copper(II) and zinc(II) ions from aqueous solutions by batch operates. The removal efficiencies of lead(II), copper(II) and zinc(II) ions of magnetic NH$_2$-MCM-41 were 88, 91 and 95%, respectively. The maximum adsorption capacities calculated from the Langmuir model were 268, 93 and 82 mg g^{-1}, respectively.

For Anbia, M. *et al.* [41], MCM-48 was composited with magnetic nanoparticles that were synthesized by chemical co-precipiation method. The prepared magnetic nanoparticle spheres were added in to the gel composition of MCM-48. The mixture containing magnetic nanoparticles was filled into an autoclave and heated for crystallization to produce magnetic-MCM-48 nanocomposites. The surface of composites were modified with (3-aminopropyl) triethoxysilane to produced magnetic-NH$_2$-MCM-48 nanoparticles. Then, the magnetic-NH$_2$-MCM-48 nanoparticles were added to the mixture contain cyanuric chloride and N,N-Diiso propylethylamine. The mixture was stirred for 1 day and reflux with ethylenediamine then soxhlet extracted with tetrahydrofuran to produce a magnetic-melamine-based dendrimer amines-MCM-48. MDA-mag-MCM-48 exhibits a Type IV profile according to the BET classification, and the surface area and pore size of MDA-mag-MCM-48 were 511 m^2/g and 3.46, respectively. The lead adsorption capacity of MDA-mag-MCM-48 were 127.24 mg/g.

The literature review showed that amino group and thiol group exhibit a good efficiency to adsorb lead ion with coordinated covalent. SBA-15 is a better supporter than MCM-41 with the same APTES ligands and DETA ligand. An increase in number of amino group in the molecule could lead to higher efficiency of lead adsorption when comparing DETA with APTES ligand.

In this work, SBA-15 and MCM-48 prepared using hydrothermal methods were used as adsorbents with large surface area. Diethylenetriamine and 2-aminothiophenol, with amino and mercapto group, modified mesoporous silicas were prepared and studied as adsorbent for removal of lead ions. Moreover, for the preparation of iron oxides nanoparticle-mesoporous silica nanocomposites, magnetic nanoparticles have been introduced into the sorbents because they can facilitate rapid separation from aqueous solutions by a magnet.

CHAPTER 3

EXPERIMENTS

The preparation of magnetic composite of mesoporous silica for lead(II) removal was divided into 4 parts.

Part 1 : Preparation of magnetic composite of mesoporous silica

- Synthesis of MCM-48

- Synthesis of SBA-15

- Synthesis of magnetic nanoparticles

- Preparation of the composite of mesoporous silica and magnetic nanoparticles

Part 2 : Functionalization of the nanocomposites

- Functionalization of diethylenetriamine (DETA) onto magnetic composite

- Functionalization of 3-mercaptopropyltrimethoxysilane (MPTMS) onto magnetic composite

- Functionalization of 2-aminothiophenol onto magnetic composite

Part 3 : Characterization of the magnetic composite of mesoporous silica
Part 4 : Adsorption study of lead

- Effect of time
- Effect of lead solution pH
- Reusability of the composites
- Effect of foreign ions in Pb(II) removal operation

3.1 Apparatus

- Fourier transform infrared spectroscopy (FT-IR) were measured using the Impact 410 (Nicolet).

- X-ray diffraction (XRD) were measured using the DMAX 2200/Ultima (Rigaku).

- Surface area analyzer were measured using the BELSORP-mini (BEL Japan).

- Scanning electron microscopy (SEM) were measured using the JSM-54 10LV (JOEL).

- Transmission electron microscopy (TEM) were measured using the JEM-2100 (JOEL).

- Thermogravimetric analysis (TGA) were measured using the Pyris 1 TGA (Perkin Elmer).

- Flame atomic absorption spectrometer (FAAS) were measured using the Analyst 100 (Perkin Elmer).

3.2 Chemicals and reagents

All chemicals were used without purification

3.2.1 Chemicals

Table 3.1 List of chemicals

Chemicals	Suppliers
Cetyltrimethylammonium bromide (CTAB)	Sigma–Aldrich
Tetraethoxysilane (TEOS)	Sigma–Aldrich
Pluronic® P-123	Sigma–Aldrich
3-mercaptopropyltrimethoxysilane (MPTMS)	Sigma–Aldrich
3-chloropropyltrimethoxysilane (CPTMS)	Sigma–Aldrich
Diethylenetriamine (DETA)	Sigma–Aldrich
1000 g/mL of lead standard solution	Sigma–Aldrich
1-ocadecene	Sigma–Aldrich
Toluene (99%)	Merck
Hexane	Merck
Absolute ethanol	Merck
Sodium hydroxide (99%)	Merck
Oleic acid	Merck
Hydrochloric acid (conc.)	Merck
Chloroform	Merck
Toluene	Merck
Nitric acid (conc.)	Merck
Iron (III) chloride ($FeCl_3$)	Fisher Scientific
2-aminothiophenol	Alfar aesar
3-(triethoxysilyl)propyl isocyanate (TEPIC)	Alfar aesar

.

3.3 Preparation of the magnetic composites of mesoporous silica

3.3.1 Synthesis of MCM-48

MCM-48 mesoporous silica was synthesized following a method described by Gies *et al.* with some modifications [42]. The reaction mixture with the molar ratio of 1 (TEOS):0.48 (CTAB): 0.48(NaOH): 55 (H_2O) was prepared. CTAB was added into deionized water while stirring until the solution became clear. NaOH was added into the solution under continuous stirring for 15 min. TEOS was added drop-wise to the solution under continuous stirring, and the mixture was heated at 40-50 °C for 3 h. The gel was placed in a Teflon container, then sealed and placed in an oven at 90 °C for 4 days to yield MCM-48. The product was filtrated, washed repeatedly with deionized water and dried at room temperature. Finally the samples were calcined at 540 °C for 5 h to remove the templates.

3.3.2 Synthesis of SBA-15

4.0 g of Pluronic P123 was dissolved in 30 g of deionized water and 120 g of 2 M HCl solution with stirring at 35 °C until the solution became clear. Then 8.50 g of TEOS was added into that solution with stirring at 35 °C and the mixture was aged at 80 °C for 24 h. The gel was placed in a Teflon container, then sealed and crystallized in an oven at 100 °C for 1 day. The product was filtrated, washed repeatedly with deionized water and dried at room temperature. Finally the samples were calcined at 540 °C for 5 h to remove the templates [43].

3.3.3 Synthesis of magnetic nanoparticles

In order to prepare MNPs, we started with the preparation of iron-oleate as precursor. 0.96 g NaOH was dissolved in 10 mL Milli Q water. Then NaOH solution was added to 7.6 mL oleic-acid in a 250 mL round bottom flask. Sodium oleate and FeCl$_3$ were dissolved in a mixed solvent containing 28 mL hexane, 16 mL ethanol, and 12 mL Milli Q water. The mixture was refluxed at 70 °C for 4 h. After refluxed, the mixture was washed three times in a separation funnel with 6 mL de-ionized water. Hexane was removed by evaporation. The iron-oleate complex was obtained in a waxy solid form.

MNPs were synthesized using thermal decomposition technique. Oleic acid (0.57 g) and iron-oleate complex (3.6 g) were added to 20 g of 1-octadecene. The mixture was slowly heated to 320 °C with a rate of 3.3 °C/min and maintained for 30 min to generate iron oxide nanocrystals using a temperature controller. After heating, the mixture was cooled to room temperature naturally. The brownish-black products were separated from the mixture via centrifugation and precipitated using ethanol to produce MNPs [44].

3.3.4 Preparation of composite of mesoporous silica and magnetic nanoparticles

MNPs were dispersed in hexane. Then the mixture was added to mesoporous silica. The mixture was stirred for 4 h at room temperature. After stirring, hexane was removed using a rotary evaporator. The brown solid was washed with hexane and dried overnight [15].

For determination of quantity of MNPs in the final composites, 10 mg of MNPs@ mesoporous-silica were digested with 50 mL of aqua regia (nitric acid and hydrochloric acid in the volume ratio of 1:3 and heat at 100 °C for 24 h until the metal oxides were totally dissolved [45]. The final concentration of Fe ion was determined by FAAS.

3.4 Functionalization

3.4.1 Functionalization of diethylenetriamine (DETA) onto magnetic composite

For the functionalization of MNPs@mesoporous-silica with DETA, we adopted the process previously reported with some modification [39]. 0.5 g of MNPs@mesoporous-silica was pretreated at 100 °C for 1 h and then added into 10 mL toluene. Then, 1 mL CPTMS was added into solution as shown in Scheme 3.1. The mixture was refluxed under nitrogen atmosphere for 4 h. The chloro-functionalized product was filtrated then washed with ethanol and oven-dried at 100 °C for 1 h. Then the precipitate was added into 10 mL of toluene. 1 mL DETA was added to chloro-product under refluxed for 18 h under nitrogen flow. The amino-functionalized product was filtrated and then washed with ethanol and oven-dried at 100 °C for 1 h to produce DETA-MNPs@ mesoporous silica as shown in Scheme 3.2.
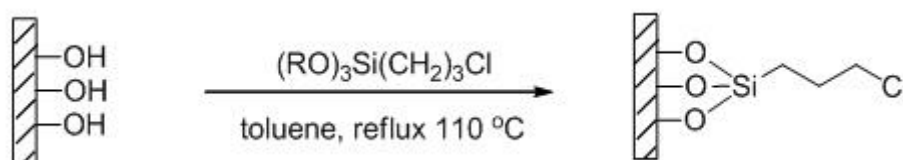
Scheme 3.1 Functionalization of MNPs@mesoporous-silica using 3-chloropropyltrimethox-silane (CPTMS)
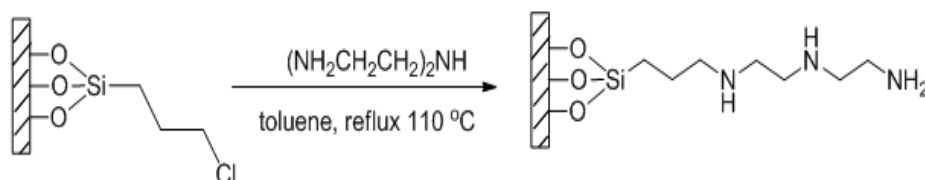
Scheme 3.2 Functionalization of MNPs@mesoporous-silica using diethylenetriamine (DETA)

3.4.2 Functionalization of 3-mercaptopropyltrimethoxysilane (MPTMS) onto magnetic composite

For thiol-functionalized MNPs@mesoporous-silica, we used the process previous reported with some modifications [46]. Typically 0.5 g of MNPs@mesoporous-silica was pretreated at 100 °C for 1 h. Then MNPs@mesoporous-silica was added into 30 mL toluene, and 1.96 mL MPTMS was added to the reaction mixture. The mixture was refluxed under nitrogen atmosphere for 5 h. After refluxed, the thiol-functionalized product was filtrated then washed with ethanol and oven-dried at 120 °C for 16 h to produce SH-MNPs@mesoporous-silica as shown in Scheme 3.3.
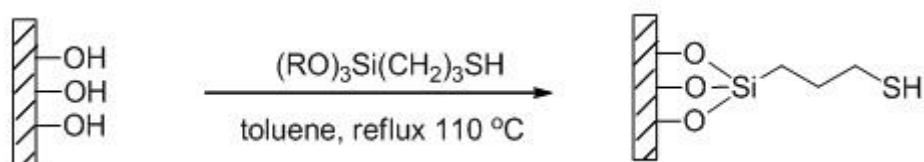
Scheme 3.3. Functionalization of MNPs@mesoporous-silica using 3-mercaptopropyltrimethoxy- silane (MPTMS)

3.4.3 Functionalization of 2-aminothiophenol (AMTP) onto magnetic composite

0.5 g MNPs@mesoporous-silica was added into 20 mL chloroform. Then, 2.5 mL TEPIC was added into solution (Scheme 3.4). The mixture was refluxed under nitrogen atmosphere for 16 h. The TEPIC product was washed with chloroform and dried at ambient temperature. The TEPIC product was added into 20 mL chloroform. 1.07 mL 2-aminothiophenol was added to TEPIC product under refluxed for 16 h under nitrogen flow (Scheme 3.5). The 2-aminothiophenol product was filtrated then washed with chloroform and dried at ambient temperature to produce 2-aminothiophenol-MNPs@mesoporoussilica.
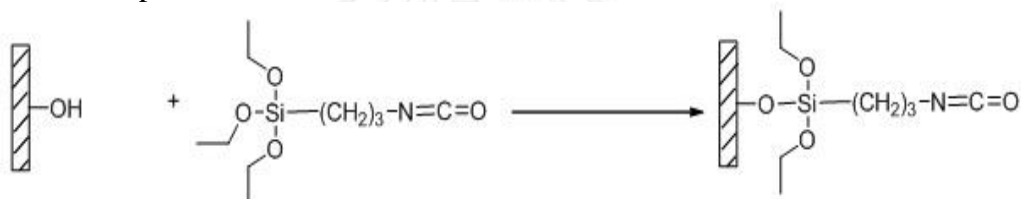
Scheme 3.4 Functionalization of MNPs@mesoporous-silica using 3-(triethoxysilyl)propyl isocyanate (TEPIC).
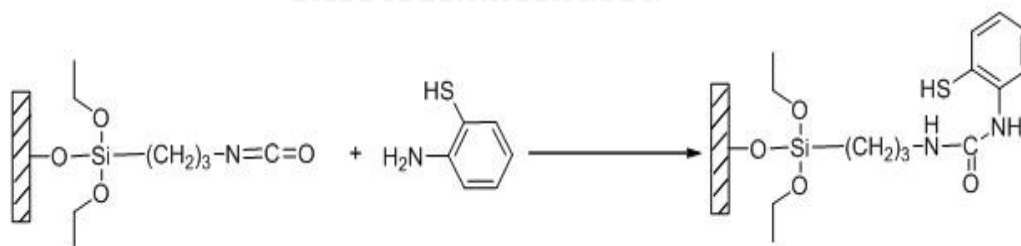
Scheme 3.5 Functionalization of MNPs@mesoporous-silica using 2-aminothiophenol (AMTP).

3.5 Characterization

The confirmation of crystalline magnetic composite of mesoporous silica phase obtained was done using X-ray diffractometer. The XRD patterns of mesoporous silica and Fe_3O_4 were scanned at 2θ in ranges of 2 to 8 and 20 to 70, respectively.

To determine the Nitrogen adsorption–desorption isotherms, surface area and pore diameter, the measurement was done using a surface area analyzer.

Scanning electron microscope (SEM) and transmission electron microscope (TEM) were used to determine the morphology of the synthesized particles.

The stability of mesoporous silica and functionalized-MNPs@mesoporous-silica at high temperature were studied by Thermo gravimetric analysis (TGA).

The surfaces of the mesoporous silica before and after functionalization were characterized by FT-IR.

Ninhydrin (2,2-Dihydroxyindane-1,3-dione) test and Ellman (5,5'-dithio-bis-(2-nitro benzoic acid)) test were used to detect primary amines and thiol groups in the modified samples.

3.5.1.Ellman test

The Ellman reagent (5,5'-dithio-bis-(2-nitrobenzoic acid), DTNB) was prepared by dissolving 40 mg DTNB in 10 mL DMSO. Then the solution was diluted 100 fold by 0.1 M Tris-HCl pH 7.5 to make DTNB working solution. DTNB working solution was added to the thiol samples and incubated at room temperature for 2 min. DTNB reacts with a free sulfhydryl group to produce a mixed disulfide and 2-nitro-5-thiobenzoic acid (TNB). TNB showing a yellow color in the mixture indicates that the samples contain thiol groups [45].
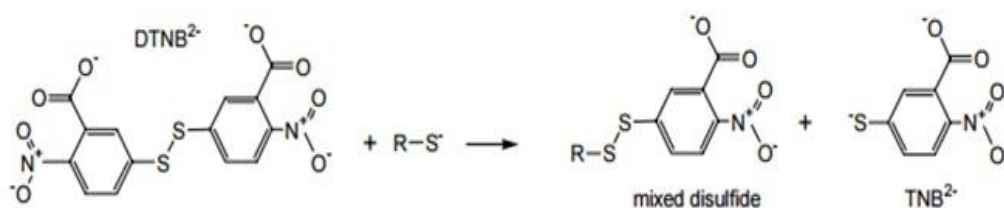
Scheme 3.6 Schematic presentation of the mechanism of Ellman reagent reacting with thiol group.

3.5.2 Ninhydrin test

The ninhydrin reagent (2,2-Dihydroxyindane-1,3-dione) is normally used as a reagent that reacts with primary amine. The nindydrin reagent was prepared by dissolving ninhydrin in ethanol to produce ninhydrin working solution. It was added dropwise onto amine samples. Then, NH_2-MNPs@mesoporous silica samples were tested with ninhydrin working solution, and the mixture of ninhydrin and the sample was heated for 1 min. The purple color of 2-(1,3-dioxoindan-2-yl)iminoindane-1,3-dione as shown in Scheme 3.7 indicating the existence of primary amine on the NH_2-samples is observed [46].
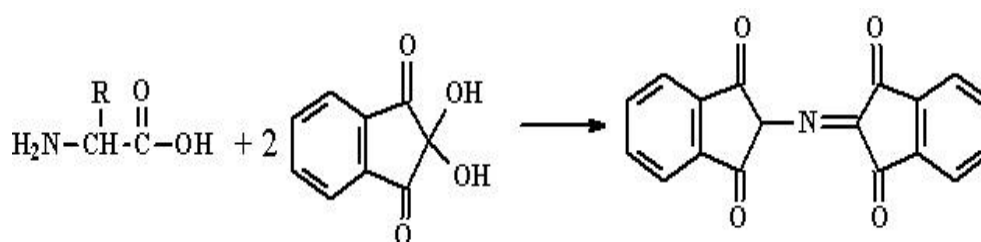
Scheme 3.7 Schematic presentation of the mechanism of Ninhydrin reagent reacting with amine group.

3.6 Adsorption study of lead

Lead adsorption experiments

The adsorption of Pb(II) onto functionalized and non-functionalized MNPs@mesoporous-silica was studied by a batch operation. Batch sorption experiments were performed using 0.02 g of absorbent in 25 mL of 10-500 mg/L Pb(II) solution at 30 °C. The pH of the solutions was adjusted using HNO_3 (1, 5 and 10 % v/v) or NaOH (1, 5 and 10 % w/v). The mixture was stirred for 2 h. The solid was separated from solution using filtration. Metal concentration, both in the initial and final solutions, was determined using FAAS.

The removal efficiency, R (%), was determined using Eq.(3.1), where C_0, and C_e are the initial and final concentrations (mgL^{-1}), respectively.

$$Sorption\% = \frac{C_0 - C_{eq}}{C_0} \times 100\%$$

3.1)

The adsorption capacity is calculated using the following Eq. 3.2;

$$q_e = \frac{C_0 - C_e}{W} V$$

<div align="right">3.2)</div>

C_0 and C_e (mg/g) are the initial concentrations and equilibrium concentrations of the Pb(II), respectively. V is the volume of the solution (cm^3), and W is the mass of sorbent (g) used.

3.6.1 Effect of initial lead concentration

The initial lead concentration was studied in the range of 10 to 500 ppm at pH 5 and 30 °C. The contact time in this experiment was fixed at 2 h.

3.6.2 Effect of lead solution pH

The pH of the solutions was adjusted using HNO$_3$ $\left(1, 5 \text{ and } 10 \text{ %v/v}\right)$ or NaOH $\left(1, 5 \text{ and } 10 \text{ %w/v}\right)$. The pH was varied at 1, 3, and 5. The effects of pH were investigated at 30 °C for 2 h.

3.6.3 Effect of adsorption time

Lead solution $\left(200 \text{ mg/L}\right)$ was in contact with the adsorbents for 15 to 240 min at 30 °C. The pH value in the experiments was fixed at 5.

3.6.4 Reusability of the sorbents

The reusability of the sorbents was investigated after the sorbents were used in lead adsorption experiments by a batch operation. Typically 0.02 g of absorbent was stirred in 25 mL of 100 mg/L Pb(II) solution at pH 5 and 30 °C for 2 h. The mixture was separated by centrifugation. Lead solution after adsorption experiments was kept in plastic bottles. After centrifuged, the used sorbents were washed using 1 M HCl. HCl solution was separated from the used sorbents again by centrifugation. Then, the sorbents were washed with DI water for 1 h. The used sorbents were dried at ambient temperature and used in another lead adsorption and reusability experiments at the same condition.

3.6.5 Effect of foreign ions in Pb(II) removal operation

Waste water samples were prepared by adding various metal ions into lead solutions. In each experiment, 0.02 g sorbents was added into 25 mL mixture containing Cd^{2+}/Pb^{2+}, Cr^{3+}/Pb^{2+} and Zn^{2+}/Pb^{2+}. The initial concentrations of Cd^{2+}, Cr^{3+}, Zn^{2+}, and Pb^{2+} ions were fixed at 100 mg/L. Then the mixtures were stirred for 2 h at room temperature. After stirred, the sorbents were filtrated, and the final Cd^{2+}, Cr^{3+}, Zn^{2+}, and Pb^{2+} ions concentrations were determined using FAAS.

CHAPTER 4

RESULTS AND DISCUSSION

Part 1 Preparation of magnetic composites of mesoporous silica

4.1 Characterization of MCM-48, SBA-15 and functionalized MNPs-MCM-48, MNPs-SBA-15

4.1.1 X-ray diffraction

The confirmation of crystalline MCM-48, SBA-15, MNPs@MCM-48, and MNPs@SBA-15 phases obtained was done using an X-ray diffractometer. The low and high angle XRD patterns of sorbents were attributed to the peaks of the mesoporous materials and the magnetic nanoparticles, respectively.
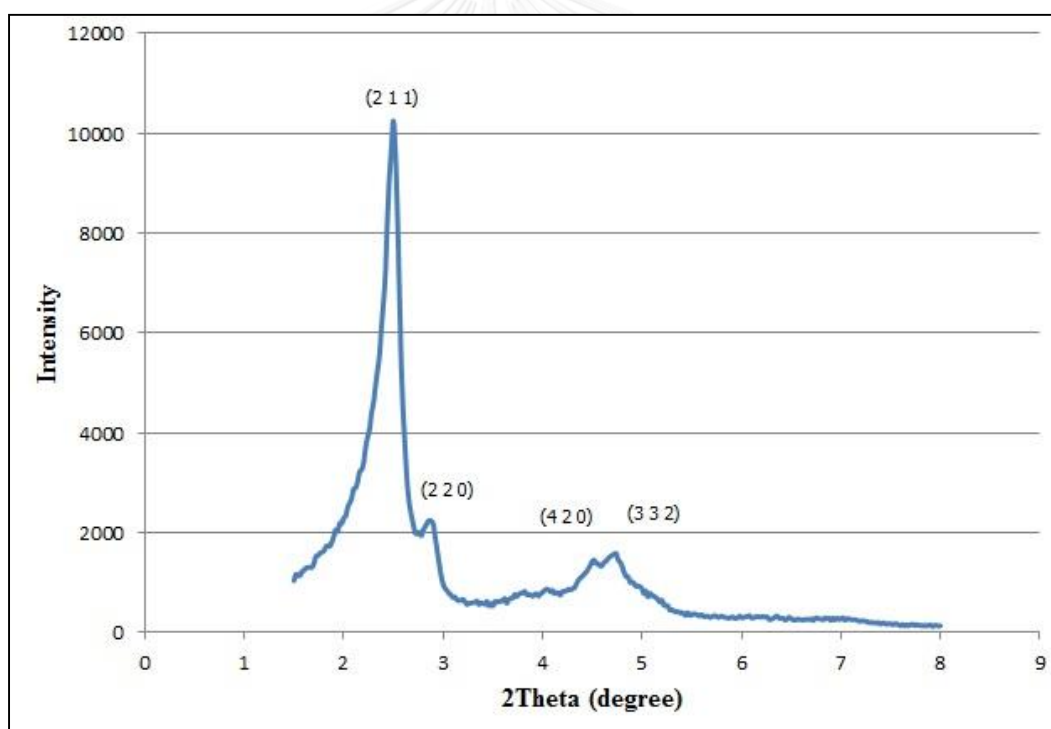
Figure 4.1 X-ray diffraction pattern of MCM-48.

The XRD pattern of MCM-48 (Figure 4.1) showed a dominant (211) and weaker (220), (420) and (332) reflections in low diffraction angle region (2-theta = 2-8 degree). The pattern was attributed to the three-dimensional mesostructures with an Ia3d cubic space group [47].
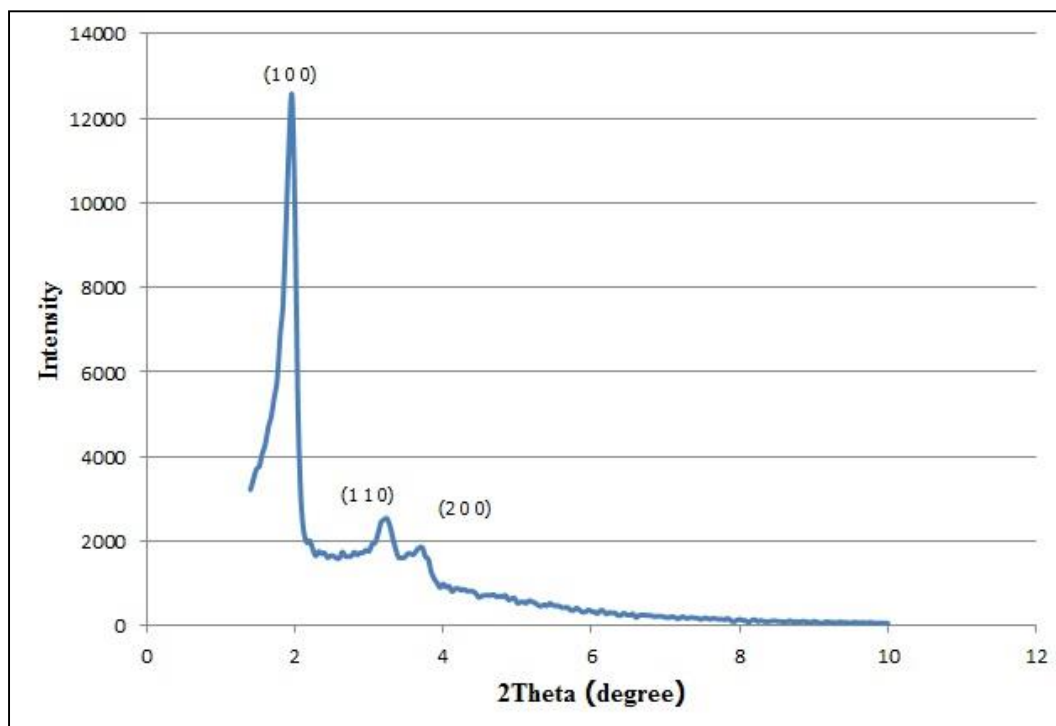
Figure 4.2 X-ray diffraction pattern of SBA-15.

The XRD pattern of SBA-15 (Figure 4.2) showed a parent peak (100) and weak peaks (110), (200) in low diffraction angle region (2-theta = 2-8 degree) attributing to the two-dimensional hexagonal mesostructures (Figure 4.2) [16].
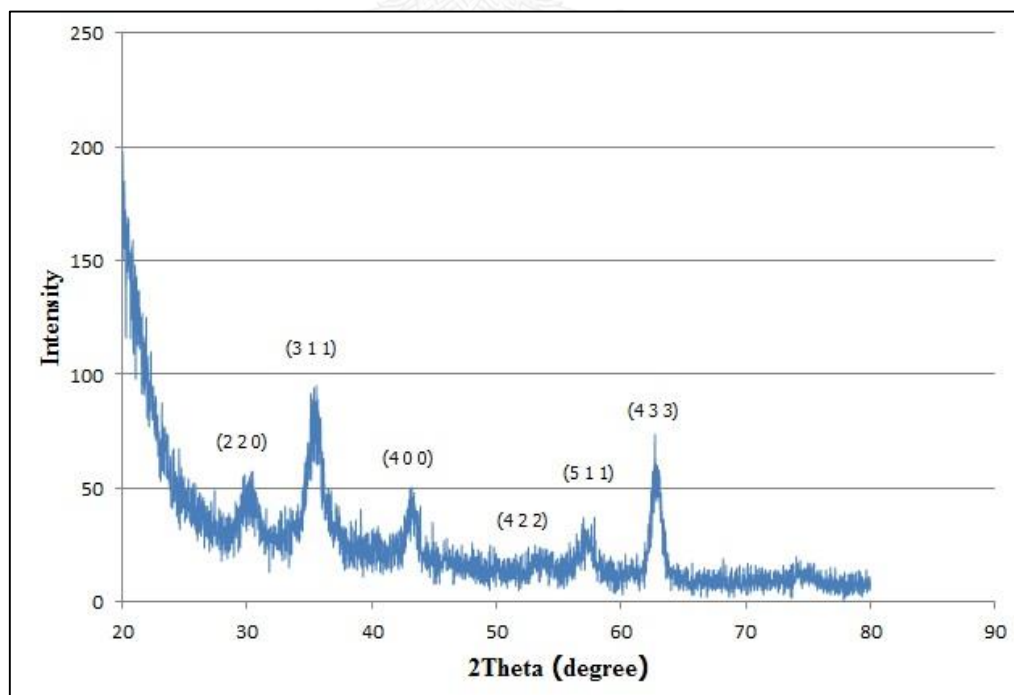
Figure 4.3 X-ray diffraction pattern of MNPs.

The XRD pattern of MNPs (Figure 4.3) was observed in high diffraction angle region (2-theta = 20-80 degree) and showed diffraction peaks at around 30.4, 35.8, 43.5, 53.8, 57.5, 63 degree. It indicates that structure of the MNPs is crystalline phase of Fe_3O_4 (JCPDS Card No. 19–0629) [48].
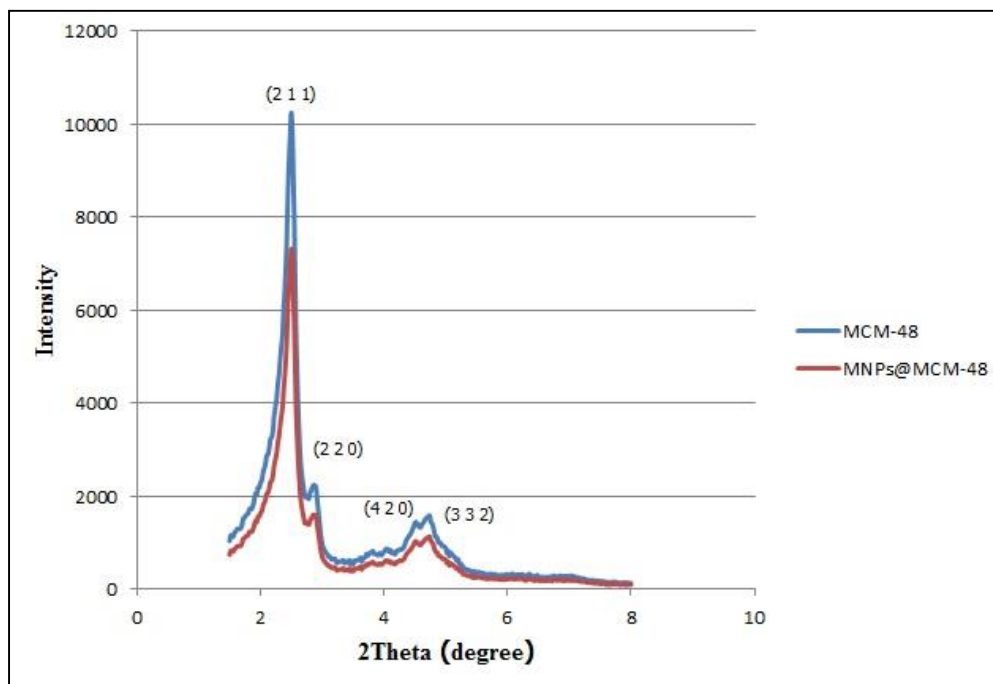
Figure 4.4 X-ray diffraction patterns of MCM-48 and MNPs@MCM-48.
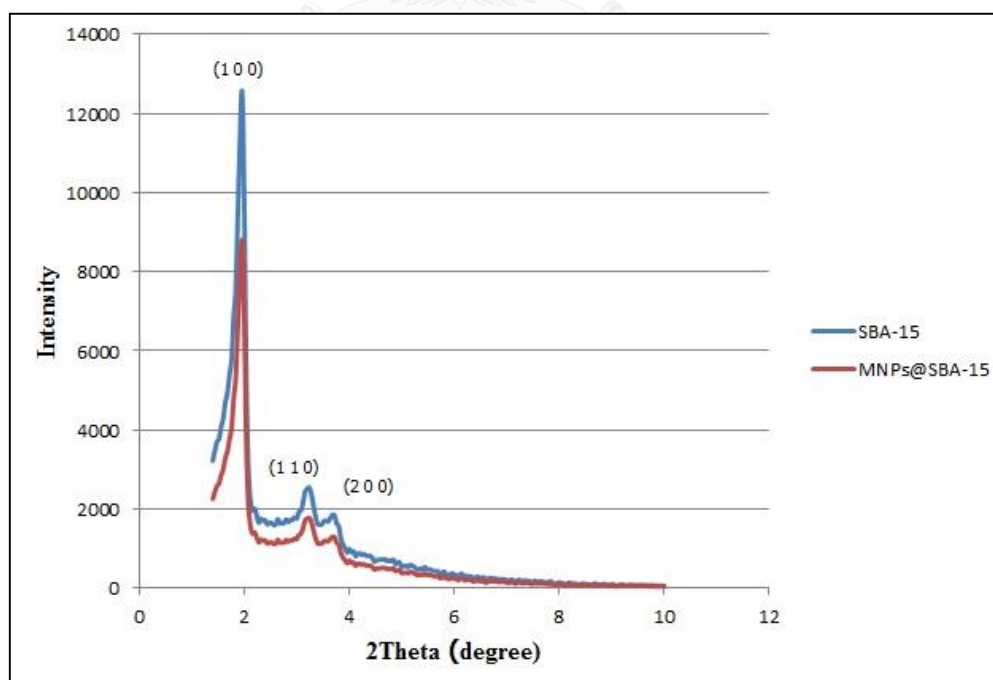
Figure 4.5 X-ray diffraction patterns of SBA-15 and MNPs@SBA-15.
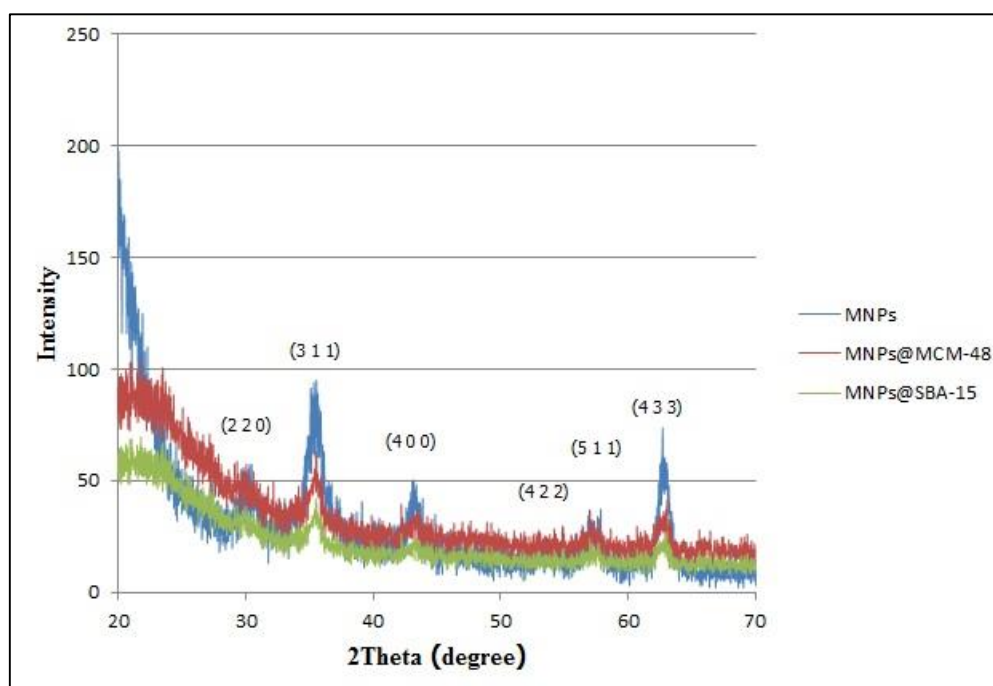
Figure 4.6 X-ray diffraction patterns of MNPs, MNPs@MCM-48 and

MNPs@SBA-15

MNPs@MCM-48 and MNPs@SBA-15 were synthesized and the phases obtained were also determined using an X-ray diffractometer. In low diffraction angle region (2-theta = 2-8 degree) the XRD pattern of MNPs@MCM-48, MNPs@SBA-15 also showed (211), (220), (420), (332) reflections, and (100), (110), (200) reflections with lower intensity compared to MCM-48 and SBA-15 (Figure 4.4 and 4.5), respectively. This result indicated that MNPs@MCM-48 and MNPs@SBA-15 still maintain the cubic and hexagonal structures after loading of magnetic nanoparticles into mesoporous silica. In high diffraction angle region (2 theta = 20-70 degree), the XRD patterns of MNPs@MCM-48 and MNPs@SBA-15 (Figure 4.6) also showed diffraction peaks at around 30.4, 35.8, 43.5, 53.8, 57.5, 63 degree indicating the existence of MNPs crystalline structure.

XRD patterns of MNPs@MCM-48 and MNPs@SBA-15 showed that the mesoporous materials contained magnetic nanoparticles in their structures. Therefore, the composites should inherit the ferrimagnetic properties of strong magnetic attraction to a magnetic field.

Moreover, we demonstrated that the magnetic nanoparticle-mesoporous silica composites exhibited magnetic responses and could be completely separated from water within 60 min under an external magnetic field as shown in Figure 4.7
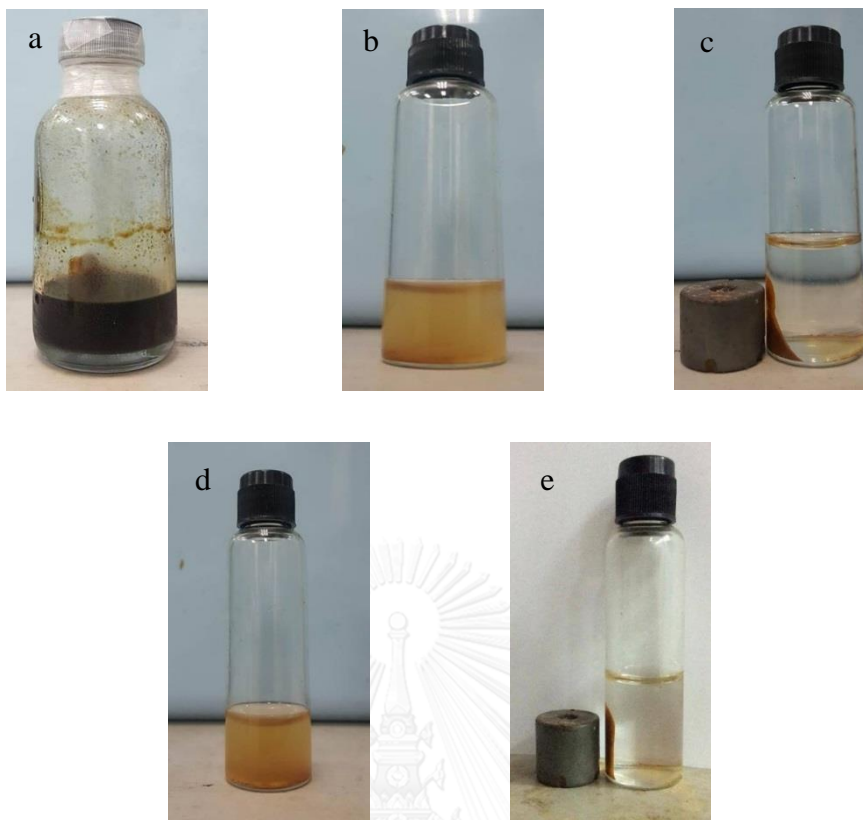
Figure 4.7 Photographs of magnetic responses of a) MNPs, b) MNPs@MCM-48 in solution before a magnetic field applied, c) MNPs@MCM-48 in solution after a magnetic field applied for 60 min, d) MNPs@SBA-15 in solution before a magnetic field applied, e) MNPs@SBA-15 in solution after a magnetic field applied for 60 min.

MNPs were added to MCM-48 and SBA-15 with 60 weight percent of MCM-48 and SBA-15. 10 mg of MNPs@MCM-48 and MNPs@SBA-15 were extracted using aqua regia to determine the amount of the magnetic particles on the MNPs@MCM-48 and MNPs@SBA-15. The final concentrations of Fe in the extracted solutions were determined by FAAS.

The observed amount of the magnetic particles in the MNPs@MCM-48 and MNPs@SBA-15 were calculated according to Eq.(4.1) and Eq.(4.2)

$$mmol\ Fe = Fe\ conc.\frac{mg}{L} \times \frac{1\ L}{1000\ mL} \times V\ of\ extrac.\ solution\ (mL) \times \frac{1}{MW\ of\ Fe\ (mg)}$$

4.1)

$$\frac{mmol\ MNPs}{g\ composite} = mmol\ Fe \times \frac{1\ mol\ magnetite}{3\ mol\ of\ Fe} \times \frac{1}{mg\ of\ composite}$$

4.2)

From the calculation based on FAAS, the quantity of the MNP particles in the MNPs@MCM-48 and MNPs@SBA-15 were 0.943 mmol/g and 1.06 mmol/g, respectively which were calculated as percent by weight of MNPs composite were 21.84 % and 24.56 %, respectively, according to Eq.(4.3)

$$\%\ by\ weight = \frac{mmol\ of\ magnetite}{g\ of\ composite} \times \frac{0.001\ mol\ of\ magnetite}{1\ mmol\ magnetite} \times \frac{MW\ of\ magnetite}{1\ mol\ magnetite} \times 100$$

4.3)

The quantity of the magnetic nanoparticles in MNPs@SBA-15 was slightly higher than MNPs@MCM-48 likely due to the larger pore sizes of SBA-15 than MCM-48 resulting in better dispersibility of MNPs into the pores of SBA-15.

4.1.2 FT-IR spectroscopy

The surfaces of the mesoporous silica before and after functionalization were characterized by FT-IR. The features of the MCM-48 and SBA-15 are a broad band between 3400 and 3200 cm^{-1} for the O-H bond stretching of the surface silanol group, signals at 1233 and 1079 cm^{-1} for Si-O-Si stretching and signals at 962 and 804 cm^{-1} for Si-O stretching (Figure 4.8) [49].
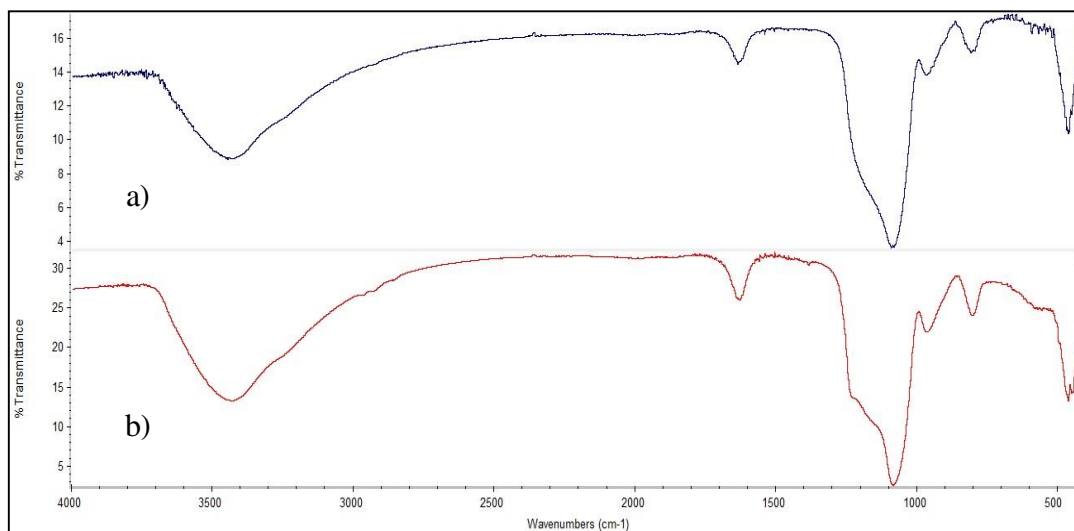
Figure 4.8 FT-IR spectra of a) SBA-15, b) MCM-48.

For the modified SH-MNP@MCM-48, SH-MNP@SBA-15, DETA-MNP@MCM-48, and DETA -MNP@SBA-15, the spectra showed C-H stretching signals at 2800-3000 cm^{-1}, 2400-2600 cm^{-1} for the thiol group [50]. However, for 3400 cm^{-1} of the amino group, which overlapped with O-H stretching, it cannot be clearly proved that the group attached on the surface (Figures 4.9 and 4.10).
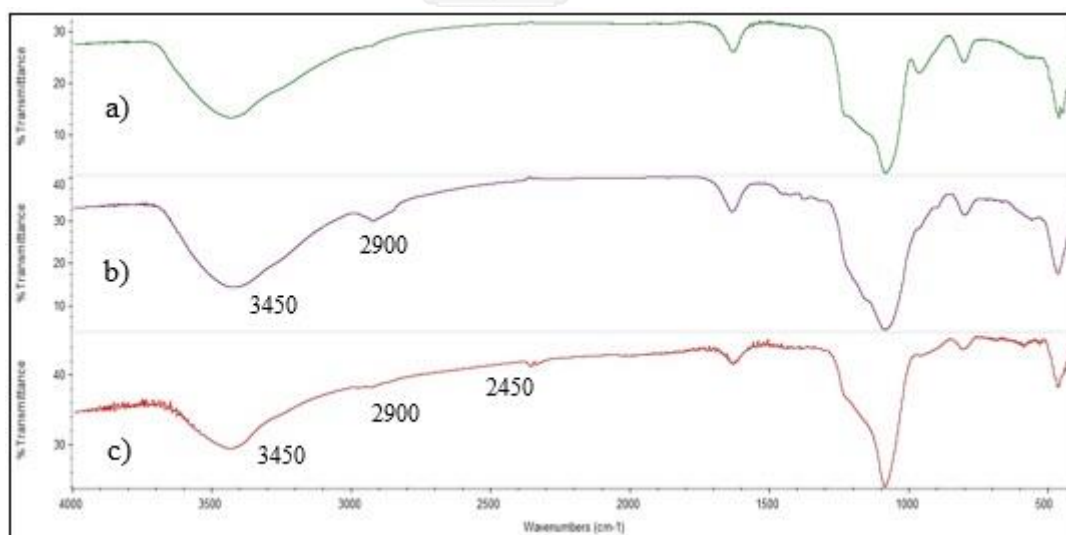
Figure 4.9 FT-IR spectra of a) MCM-48, b) DETA-MNPs@MCM-48

and c) SH-MNPs@MCM-48.
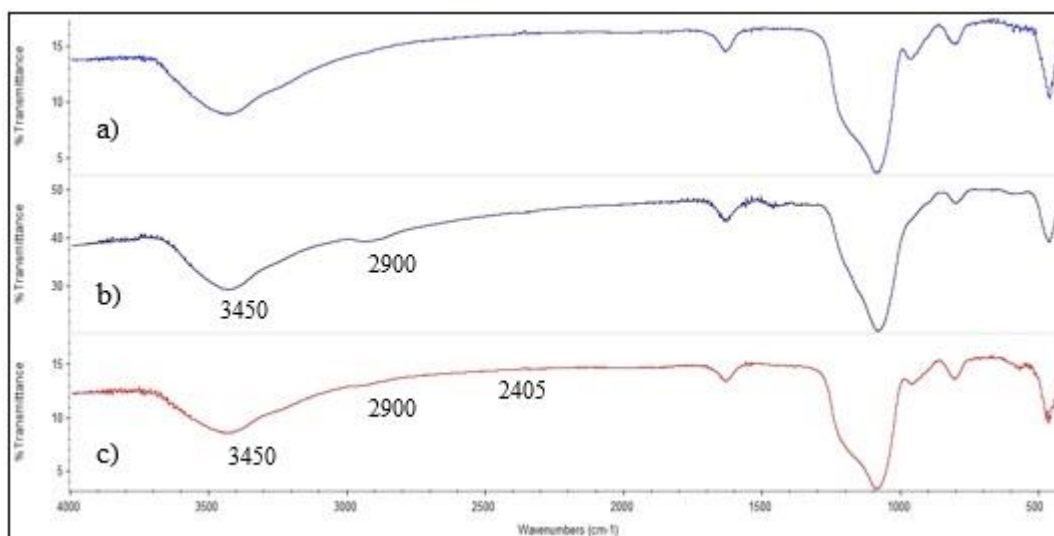
Figure 4.10 FT-IR spectra of a) SBA-15, b) DETA-MNPs@SBA-15

and c) SH-MNPs@SBA-15.

The FT-IR spectra of AMTP-MNPs@MCM-48 and AMTP-MNPs@SBA-15 showed methylene group signals at 2934 and 2853 cm^{-1}, the amide C=O stretch signals at 1686 cm^{-1} and the bending vibration at 1544 cm^{-1}, indicating the formation of amide groups onto the surface. For amino group and thiol group, the confirmative signals cannot be observed because signals of amino group overlapped with O-H stretching, and thiol groups showed weak signal around 2550-2600 cm^{-1} [51] (Figures 4.11 and 4.12).
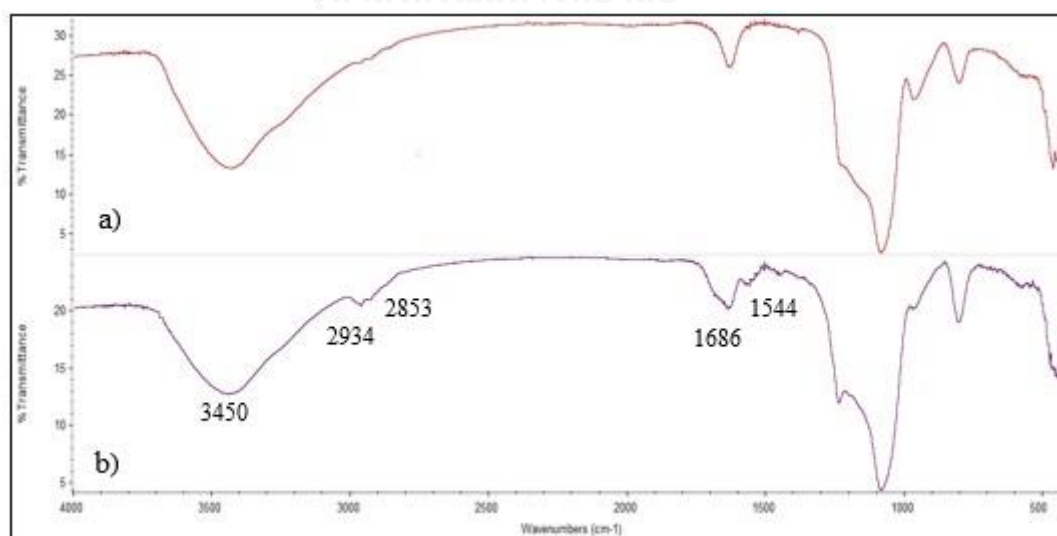
Figure 4.11 FT-IR spectra of a) MCM-48, b) AMTP-MNPs@MCM-48.
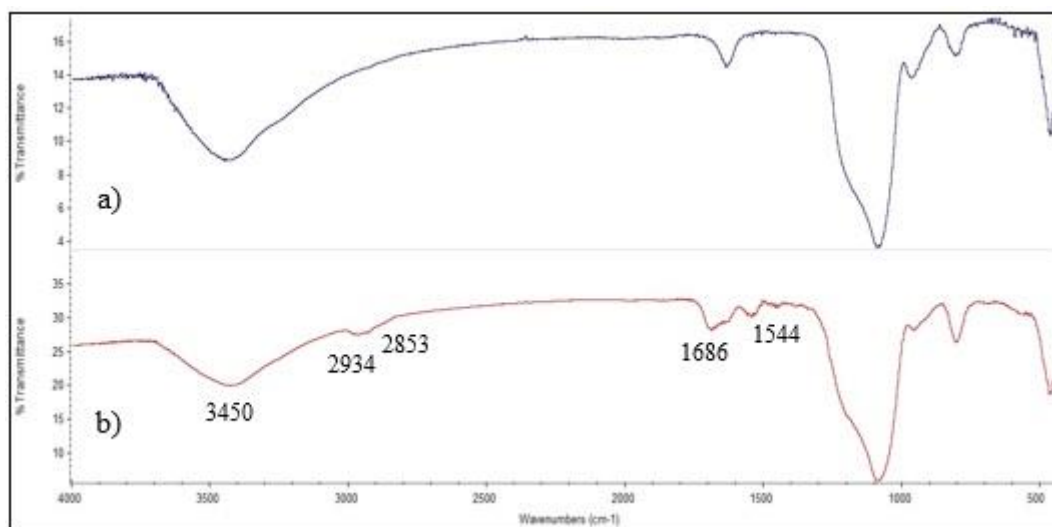
Figure 4.12 FT-IR spectra of a) SBA-15, b) AMTP-MNPs@SBA-15.

In order to confirm the existence of amino and thiol groups on the NH_2- and SH-modified mesoporous silica, ninhydrin test and Ellman test were used.

4.1.3 Ellman test

For FT-IR spectra thiol groups in the magnetic nanoparticle-mesoporous silica composites were not observed in the wavenumber about 2550-2600 cm^{-1}. Ellman test method was used to confirm the thiol group in the samples. After the DTNB working solution was added to the thiol-functionalized magnetic nanoparticle-mesoporous silica composites. The yellow color was observed in the mixtures containing SH-modified mesoporous silica indicating that the TNB^{2-} molecule was released from free sulfhydryl groups on 2-aminothiophenol. For MCM-48 and SBA-15, the yellow color was not observed in the mixtures as MCM-48 and SBA-15 do not contain free sulfhydryl in their molecules (Table 4.1).

Table 4.1 Results for Ellman test of MNPs@mesoporous silica and the thiol-
functionalized magnetic nanoparticle-mesoporous silica composites

Samples	Samples+Ellman reagent	Samples	Samples+Ellman reagent
MCM-48		SBA-15	
SH-MCM-48		SH-SBA-15	
AMTP-MCM-48		AMTP-SBA-15	
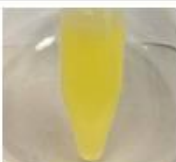
4.1.4 Ninhydrin test

Ninhydrin test was used to confirm NH_2 group on MCM-48, SBA-15, DETA@MCM-48, DETA@SBA-15, AMTP@MCM-48, and AMTP@SBA-15. In the studies, magnetite nanoparticles were not loaded into the functionalized mesoporous materials in order to avoid the false interpretation from the color of the MNPs. The mixture of samples and ninhydrin were heated, and the purple on the samples were observed（Figure 4.14）. The results showed that MCM-48 and SBA-15 were not observed to change to purple indicating that MCM-48 and SBA-15 did not contain amino groups on their surface. In contrast, for DETA@MCM-48, DETA@SBA-15, AMTP@MCM-48 and AMTP@SBA-15, the purple color can be observed on the spots of dried samples, with more intense purple on DETA@MCM-48 and DETA@SBA-15 than AMTP@MCM-48 and AMTP@SBA-15. This observation is likely due to the fact that there were more amino groups on DETA than 2-aminothiphenol or the DETA could be coated with better efficiency. The observation from ninhydrin suggested that the materials were successfully functionalized with DETA and AMTP ligands（Table 4.2）

Table 4.2 Results for ninhydrin test of MNPs@mesoporous silica and the functionalized-MNPs@mesoporous silica.

Samples	Samples + Ninhydrin reagent	Samples	Samples + Ninhydrin reagent
MCM-48		SBA-15	
DETA-MCM-48		DETA-SBA-15	
AMTP-MCM-48		AMTP-SBA-15	

4.1.5 Surface area analysis

Nitrogen adsorption-desorption analysis was used to study the surface area of the composites. Isotherms of nitrogen adsorption on MCM-48, SBA-15 and functionalized MNPsMCM-48 and MNPs-SBA-15 were classified as Type IV, confirming their mesoporous nature. The adsorption-desorption isotherms data were used to calculate the specific surface area by BET method (S_{BET}) and average pore diameter as shown in Table 4.3.
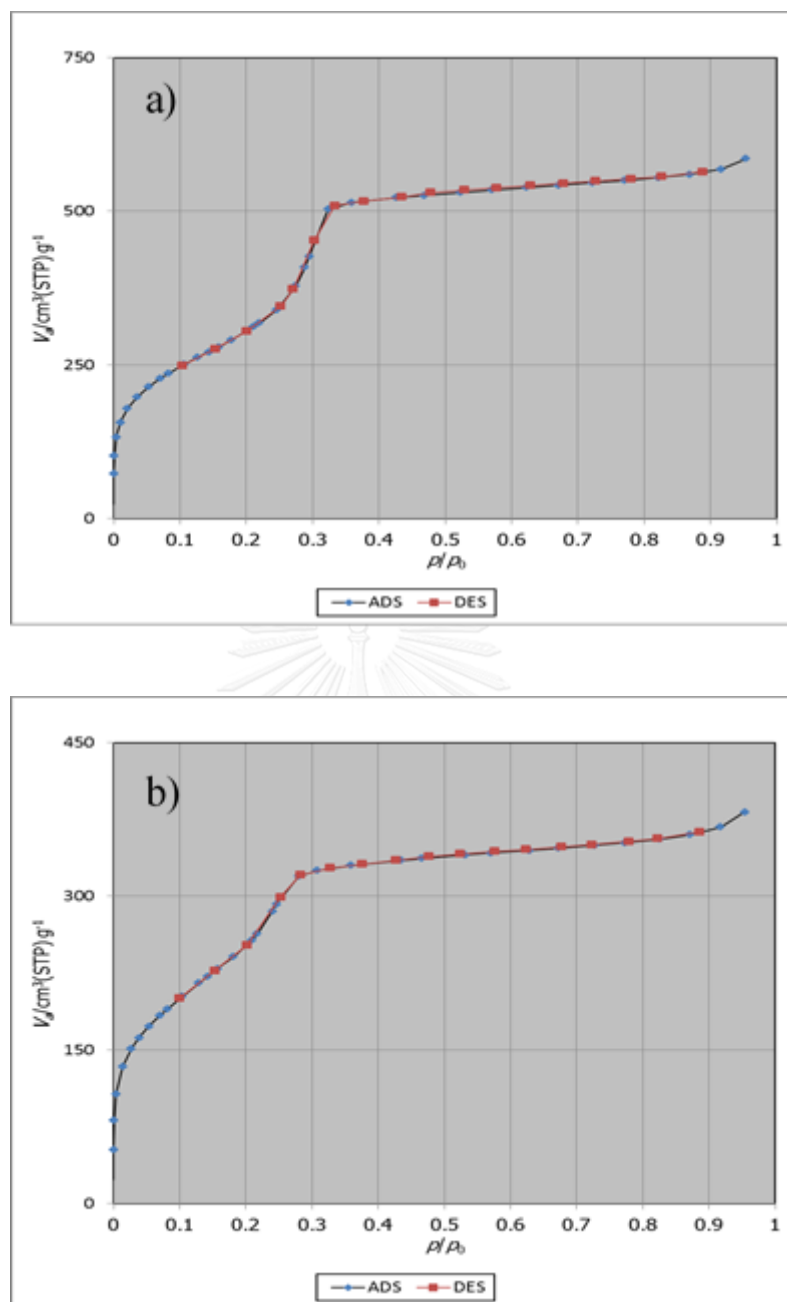
Figure 4.13 Adsorption isotherms of a) MCM-48, b) DETA-MNPs@MCM-48
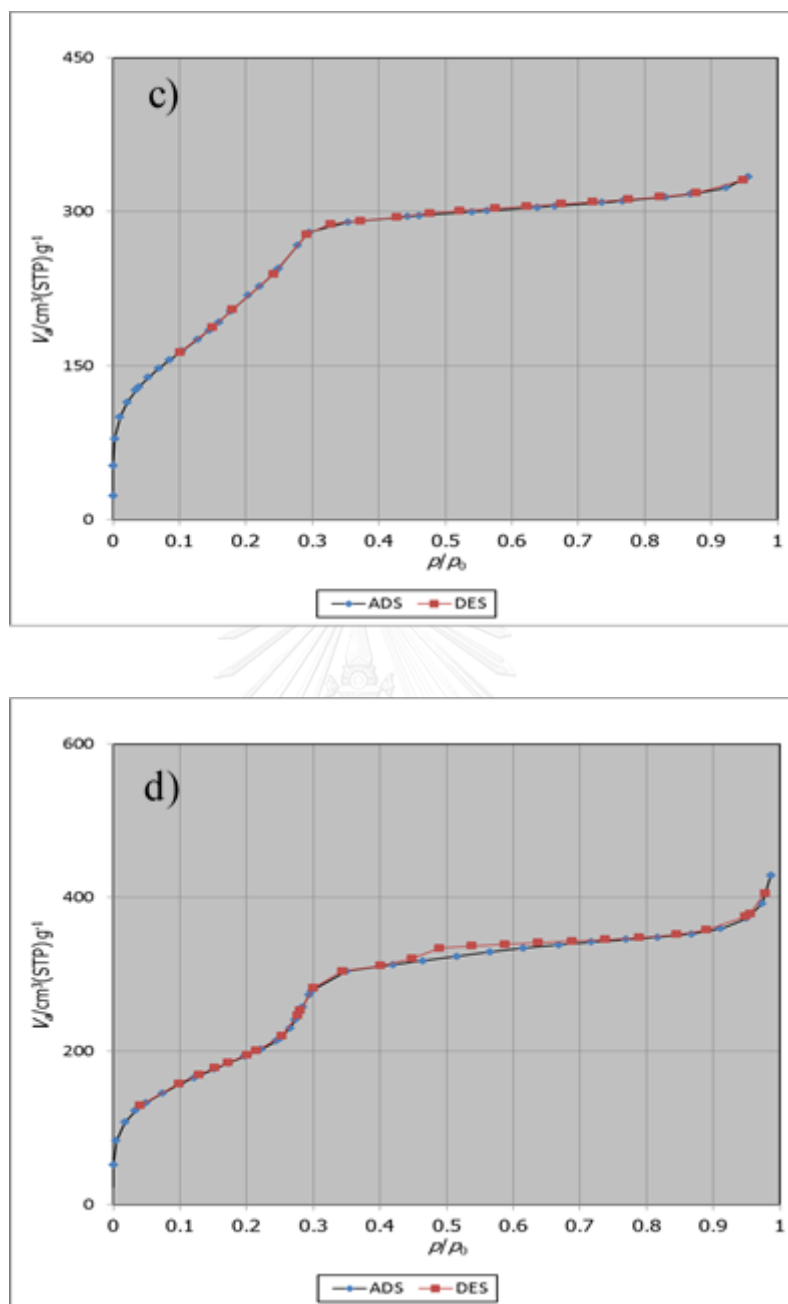
Figure 4.14 Adsorption isotherms of c) SH-MNPs MCM-48, d) AMTP-MNPs@MCM-48
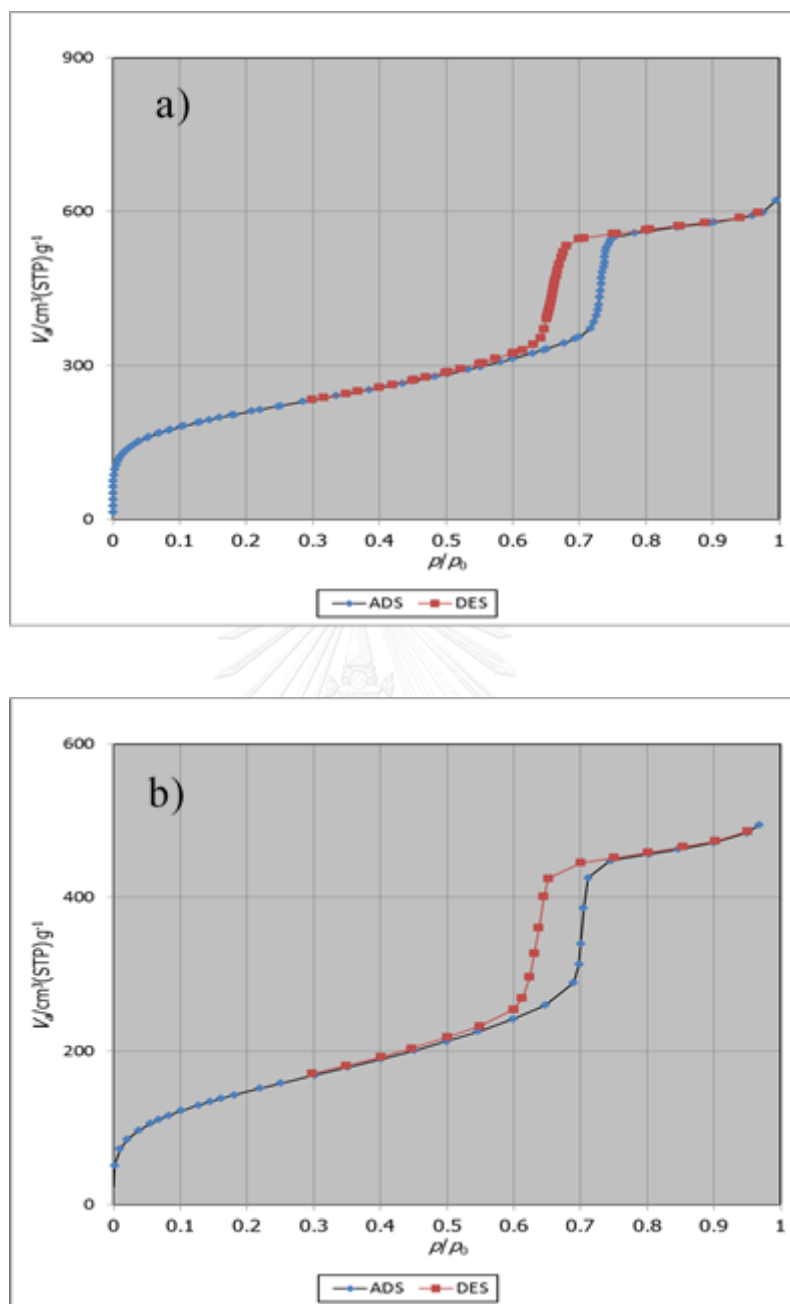
Figure 4.14 Adsorption isotherms of a) SBA-15, b) DETA-MNPs@SBA-15
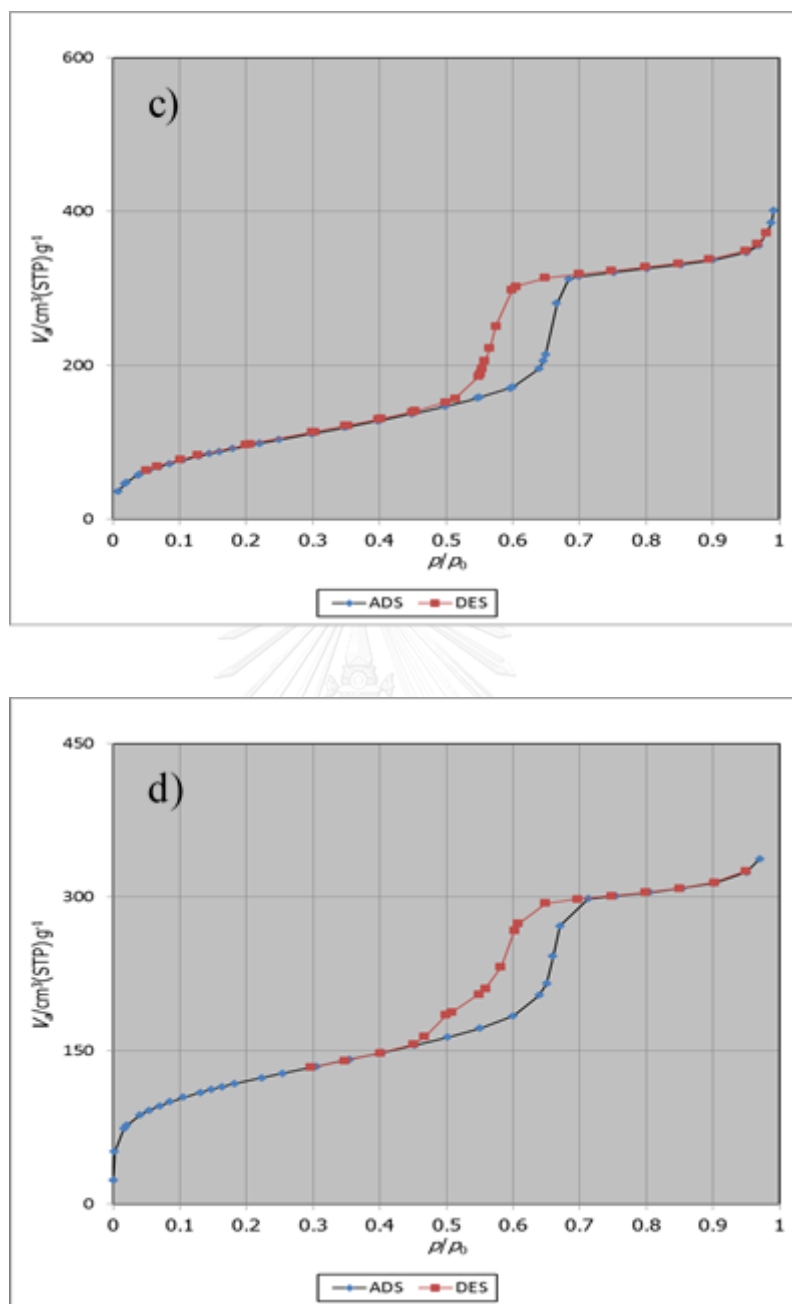
Figure 4.15 Adsorption isotherms of c) SH-MNPs SBA-15, d) AMTP-MNPs@SBA-15

Table 4.3 Surface area and pore diameter of the materials.

Materials	BET surface area (m²/g)	Average pore diameter (nm)
MCM-48	1145	2.96
DETA-MNPs@MCM-48	863	2.72
SH-MNPs@MCM-48	904	2.28
AMTP-MNPs@MCM-48	733	2.61
SBA-15	760	6.56
DETA-MNPs@SBA-15	428	5.86
SH-MNPs@SBA-15	543	5.62
AMTP-MNPs@SBA-15	363	5.67

Table 4.3 indicated that the surface area of MCM-48 was 1145 m^2/g, which was greater than that of SBA-15 (760 m^2/g), because MCM-48 materials have three-dimensional cubic structure. In other words, MCM-48 has interconnecting pore in the cubic structure, so MCM-48 materials have a high surface area when compared with the unidirectional pore SBA-15. For comparison of pore diameter between unmodified MCM-48 and SBA-15, the adsorption isotherm of SBA-15 showed a broad hysteresis loop indicating that SBA-15 contained pores of different sizes and shapes. In contrast, MCM-48 does not show any hysteresis loop resulting from the fact that SBA-15 has larger pore diameter when compared with MCM-48 [11]. Also, the isotherms of MCM-48 and SBA-15 showed a sharp increase at a relative pressure between $p/p_0 = 0.10$-0.32 and 0.3-0.7, respectively, indicating that the filling nitrogen in the channels was mainly from capillary condensation.

For the functionalized-MNPs-MCM-48 and MNPs-SBA-15, the amount of adsorbed nitrogen decreased and a value of relative pressure of the functionalized MNPs-MCM-48 and MNPs-MCM-48 were shifted down from MCM-48 and SBA-15 (Figure 4.13-4.14). Moreover, the surface area and pore diameter of the functionalized MNPs-MCM-48 and MNPs-SBA-15 exhibited lower specific surface area and pore size after modification with ligands (Table 4.3). These results implied that the pore plugging slightly occurred, and the surface area of functionalized MNPs-MCM-48 and MNPs-SBA-15 were modified or grafted by ligands. After modification with ligands, the surface area of functionalized MNPs@SBA-15 affected more than the surface area of functionalized MNPs-MCM-48 most likely because the pore sizes of SBA-15 are larger than MCM-48. As a result, and the ligand molecule could move into the pore and be grafted in the internal surface of SBA-15, while MCM-48 with the smaller pore sizes could inhibit the entering of ligands into the pores.

4.1.6 Morphology of nanocomposites by scanning electron microscopy (SEM)

Scanning electron microscopy images of MCM-48, SBA-15, MNPs@MCM-48 and MNPs@SBA-15 are shown in Figures 4.15-4.16.

The scanning electron microscope (SEM) images of pure silica MCM-48 revealed the shapes of spherical particles with 181±36 nm in diameter. The surface of MCM-48 particles are homogeneous, and an increase in surface roughness on MNPs@MCM-48 observed after the particles were loaded by MNPs, while the particle size of MNPs@MCM-48 was increased to 291±34 nm in diameter. This result may be attributed to the deposition of MNP particles on the surface of the MCM-48.

The scanning electron microscope (SEM) images of pure silica SBA-15 exhibited homogeneous rod-like shapes. The surface of MNPs@SBA-15 particles was also rougher when compared with SBA-15, and the size of SBA-15 increase from 702±119 nm to 880±121 nm in diameter after the particles were loaded by MNPs. These results may indicate that the MNPs particles experienced some aggregations on the SBA-15 materials.

These results may indicate that the MNPs particles experienced some aggregations on the mesoporous materials. From the images, it was confirmed that mesoporous silica and magnetic nanoparticles coexisted on the external surface area of the nanocomposites.
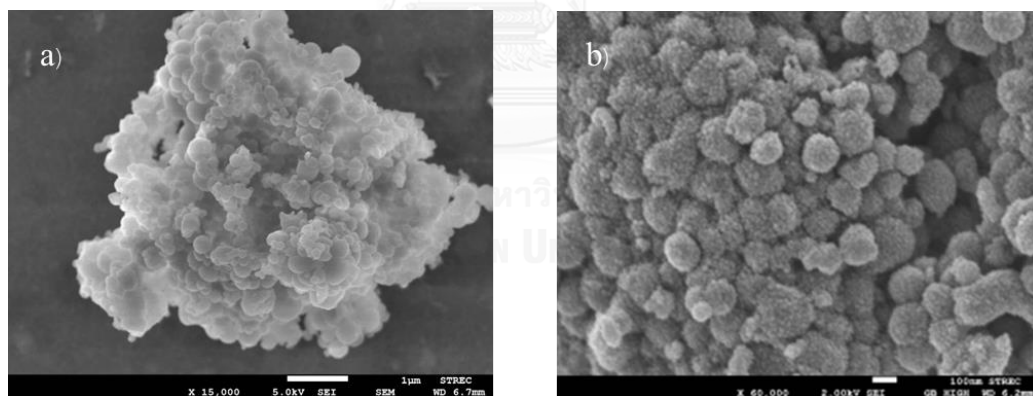
Figure 4.16 SEM images of a) MCM-48 and b) MNPs@MCM-48.
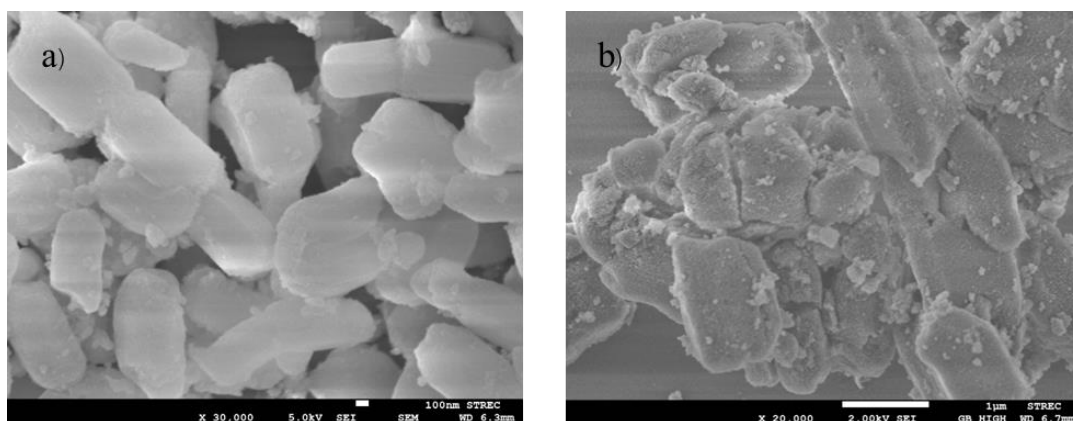
Figure 4.17 SEM images of a) SBA-15 and b) MNPs@MCM-48.

4.1.7 Morphology by transmission electron microscopy (TEM)

Transmission electron microscopy of MCM-48, SBA-15, MNP@MCM-48 and MNP@SBA-15 are shown in Figures 4.17 and 4.18.
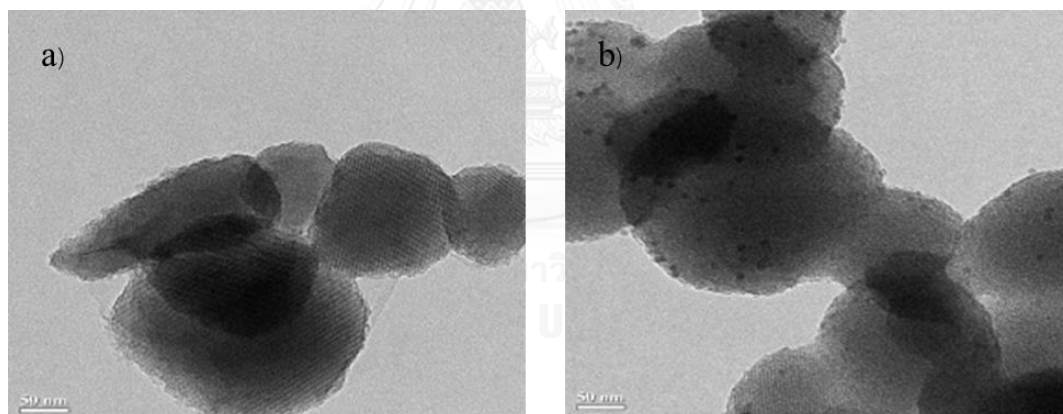
Figure 4.18 TEM images of a) MCM-48 and b) MNPs@MCM-48.
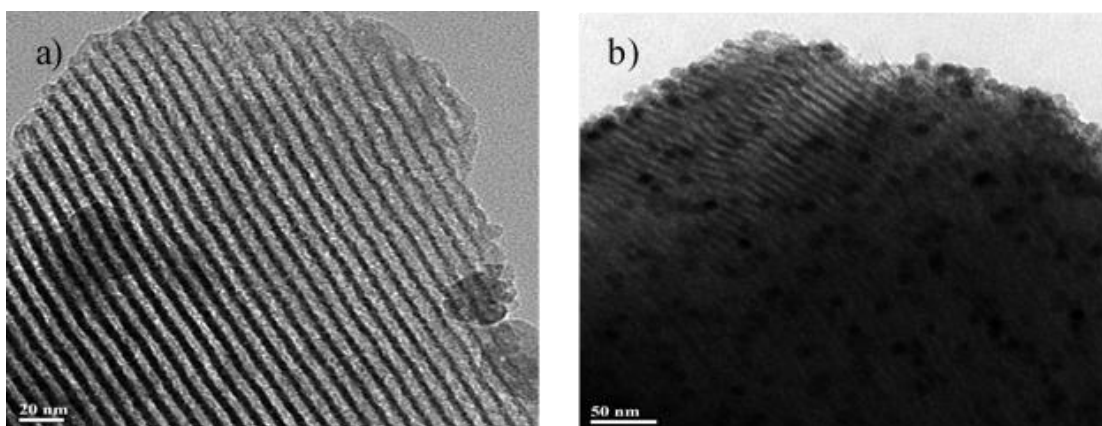
Figure 4.19 TEM images of a) SBA-15 and b) MNPs@SBA-15.

The transmission electron microscopy (TEM) images of pure MCM-48 showed the highly ordered cubic pore structure with cylindrical radial pores. After the MNPs were loaded onto the MCM-48, all of MNPs particles stayed as separate nanoparticles and appeared as dark spots inside the pore channels with good dispersity. Upon modification with MNPs, the highly ordered three-dimensional cubic mesoporous structure of MCM-48 was still observed.

The TEM images of pure silica SBA-15 showed the hexagonal array and well-ordered parallel nanotubular pores. The TEM images of MNPs@SBA-15 depicted that the MNPs also appeared as dark spots inside the pore channels and the structural ordering was still maintained after the incorporation of MNPs into SBA-15 composites.

The Fe_3O_4 nanoparticles were observed as nearly spherical particles with an average size of 10 nm. The distribution of MNPs in SBA-15 was more dispersed in the mesoporous structure than MNPs@MCM-48 due to the larger pore size of SBA-15 resulting in less hindrance from pore blocking for the MNPs to move inside the pore structure of SBA-15.

4.2 Lead Adsorption Study

4.2.1 Preliminary study

The functionalized MNPs-MCM-48 and MNPs-SBA-15 were studied for the removal of Pb(II) ion in 25 mL Pb(II) solution at 30 °C by a batch operation. The pH of lead solution was adjusted to pH 5 in order to test adsorption efficiency in each batch. 20 mg functionalized MNPs-MCM-48 and MNPs-SBA-15 were added to 400 mg/L Pb(II) solution for 2 h. The adsorption capacity and removal efficiency of the functionalized MNPs-MCM-48 and MNPs-SBA-15 are shown in Table 4.4.

Table 4.4 Adsorption capacity of the functionalized MNPs-MCM-48 and MNPs-SBA-15 at 400 mg/L.

Adsorbents	Adsorption capacity (mg/g)
DETA-MNPs@MCM-48	195.29
SH-MNPs@MCM-48	63.62
AMTP-MNPs@MCM-48	120.00
DETA-MNPs@SBA-15	139.56
SH-MNPs@SBA-15	47.65
AMTP-MNPs@SBA-15	93.00

The results indicated that the MNPs-MCM-48 and MNPs-SBA-15 modified with dietyl- enetriamine and 2-aminothiphenol performed as good sorbents for removal of lead (II) ion in solution. For dietylenetriamine containing two primary and one secondary amine groups can coordinate to lead (II) ion with nitrogen atom of each amine group, in the trivalent fashion, the chelating effects could play an important role in the stability of the DETA-Pb(II) complexes. On the contrary, 2-aminothiphenol contains only one thiol group and one amino group in a molecule resulting in the less adsorption efficiency of lead ion comparing to dietylenetriamine. For MPTMS ligand, which contains only one thiol group in a molecule, the adsorption efficiency of the materials was the least. This observation indicated that the hardness and softness in basicity of the ligands affects the adsorption capacity less than the number of binding atoms in a ligand.

Moreover, types of mesoporous materials have strong effects on the adsorption efficiency. When modified with the same ligands, MCM-48 performed as the better support materials likely due to large surface area and good pore direction with 3D dimensional pore system of MCM-48.SBA-15 possessed less surface area to modified with ligands comparing with MCM-48 leading to lower adsorption capacity.

From the preliminary results above, later on in this work, MCM-48 was chosen as support materials. MCM-48 modified with DETA and AMTP ligands was used to investigate the effects of the initial lead concentration, adsorption time and pH on the adsorption efficiency.

The reusability of the composites and the effect of foreign ions in Pb(II) removal were also investigated on the DETA-MNPs@MCM-48 and AMTP-MNPs@MCM-48. The stabilities of the two sorbents were also studied using thermal gravimetric analysis.

4.2.2 Thermogravimetric analysis (TGA)
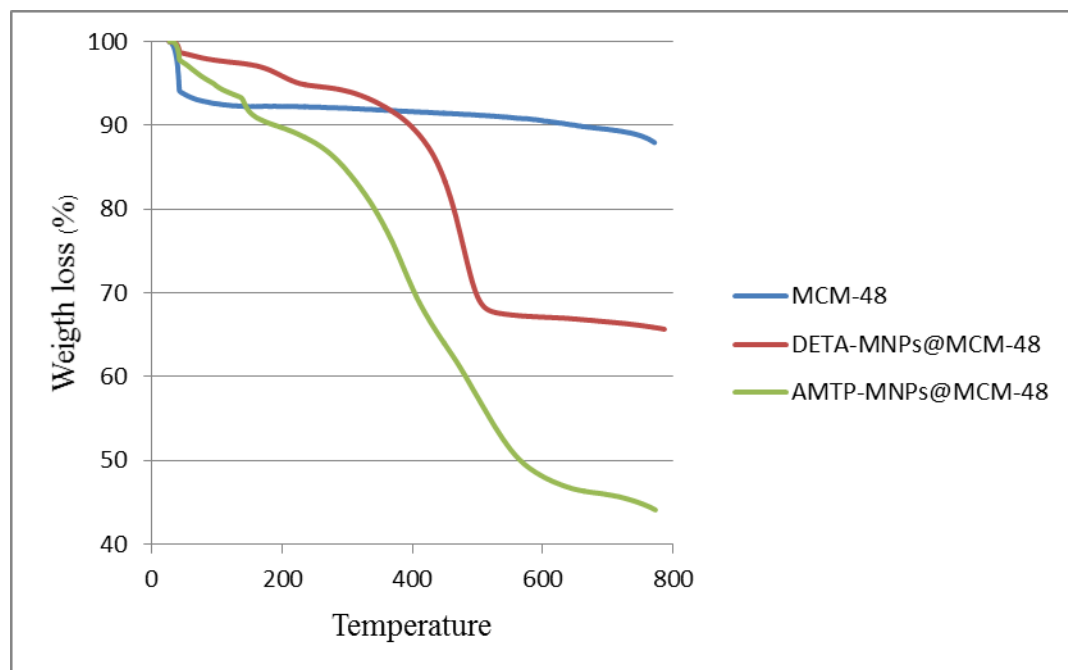
Figure 4.20 TGA curves of a) MCM-48 b) DETA-MNPs@MCM-48

and c) AMTP-MNPs@MCM-48.

From the results from TGA results, it was observed for the MCM-48 that the first weight loss peaks appeared below 100 °C which are attributed to the volatilization of the physically adsorbed H_2O and residual solvents and the MCM-48 could remain stable upon heating to 800 °C. For DETA-MNPs@MCM-48, however, there were two distinct weight loss. The first weight loss peaks around 200 °C might be due to the removal of ethanol compounds, and the second loss observed above 450 °C was likely from the decomposition of amine chains present in the silane compounds and degradation of amine compounds [52-54]. For AMTP-MNPs@MCM-48, there are three stages of weight loss. The first weight loss peaks appeared around 100 °C and 150 °C was due to moisture content in the samples and residual solvent. The loss at 375 °C was attributed to the decomposition of amine and thiol groups [55], and at 550 °C was attributed to decomposition of phenol and carbonyl groups [56, 57].

4.2.3 Effect of initial concentration of Pb(II) ion

Batch sorption experiments were performed at room temperature at pH 5. The initial concentration of lead solution was observed at the initial concentration of Pb(II) solution of 10, 50, 100, 200, 300, 400, 500 mg/L with contact time of 2 h.
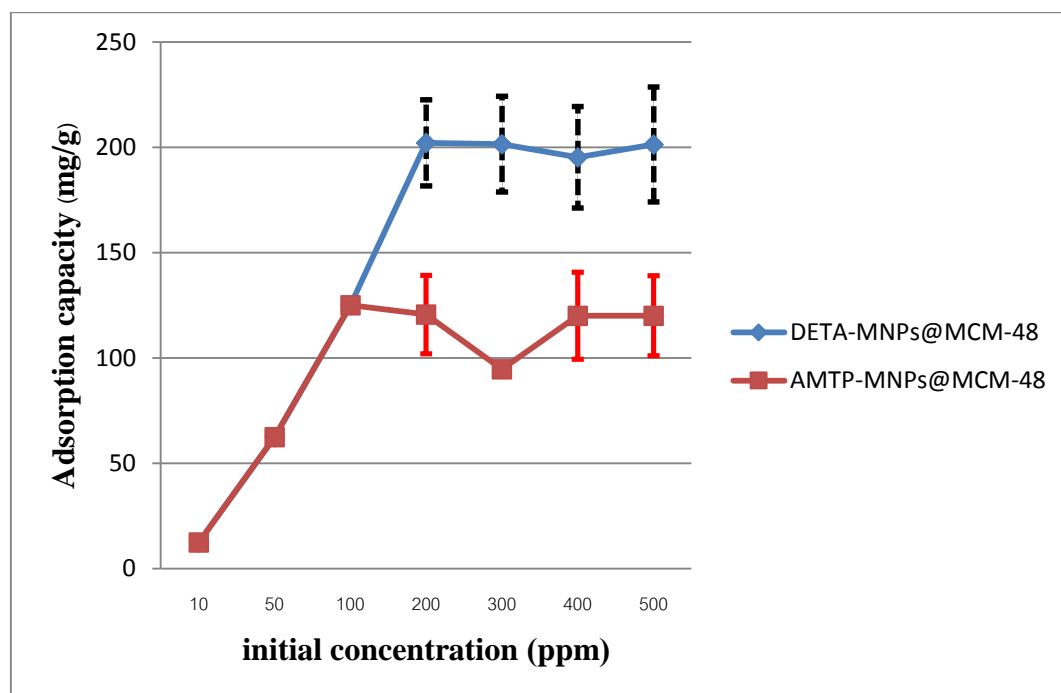
Figure 4.21 Effect of initial lead concentration on adsorption capacity of DETA-MNPs@MCM-48 and AMTP-MNPs@MCM-48 in the lead removal.
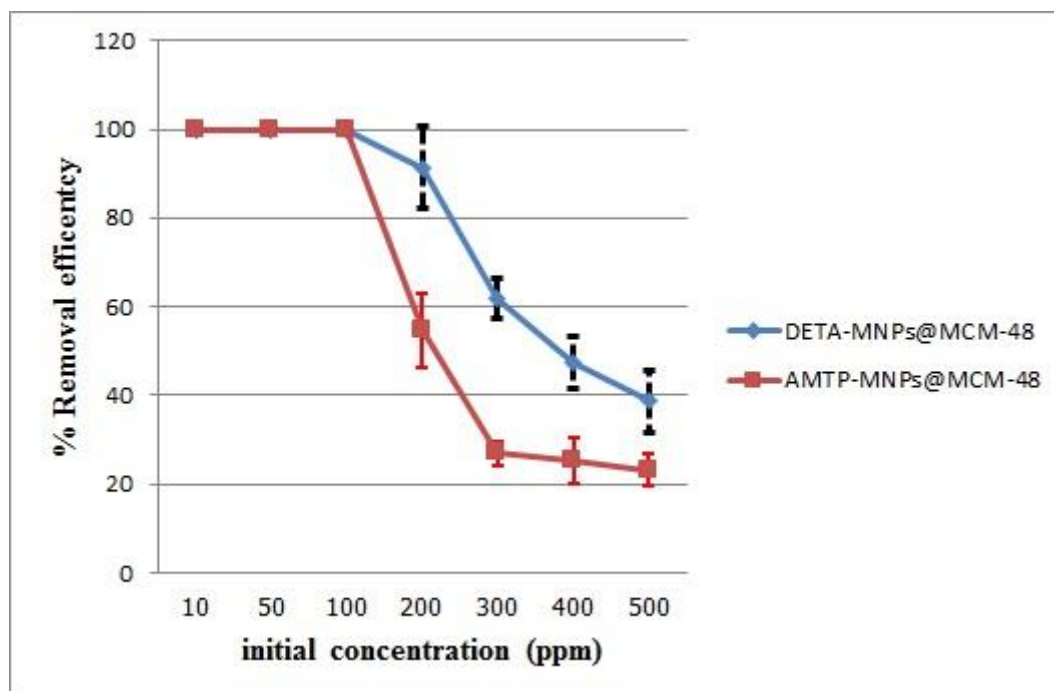
Figure 4.22 Effect of initial lead concentration on removal efficiency of DETA-MNPs@MCM-48 and AMTP-MNPs@MCM-48 in the lead removal.

The results showed that DETA-MNPs@MCM-48 and AMTP-MNPs@MCM-48 (Figures 4.20-4.21) exhibited high adsorption efficiency. The sorption of lead increased with the increase in the initial lead concentration from 10-100 ppm. The maximum capacity of DETA-MNPs@MCM-48 and AMTP-MNPs@MCM-48 were 202.13 mg/g at 200 mg/L lead solution and 125.00 mg/g at 100 mg/L lead solution, respectively. The removal efficiency of DETA-MNPs@MCM-48 and AMTP-MNPs@MCM-48 reached 100% at low initial concentration. However at higher initial lead concentration (>100 ppm), the removal efficiency decreases as the concentration of lead ion in solution reaches equilibrium due to saturation of binding sites of DETA and AMTP in the sorbents.

4.2.4 Adsorption isotherms

The data of Pb(II) adsorption were used to study the sorption isotherms of the sorbent materials. Linear plotting of the Langmuir isotherm was based on the assumption that each site can hold only one molecule. In other words, the Langmuir isotherm was calculated using adsorption in monolayer fashion only, while Freundlich model was used to describe on heterogeneous systems. The Freundlich isotherm was based on different sites with several adsorption energies are involved. The adsorption isotherms were studied at the initial Pb(II) concentration of 200-500 mg/L, pH 5.0, adsorbent dose of 20 mg : 25 mL of lead solution, and contact time for 2 h.

The Langmuir isotherm can be calculated using a linear form as shown in Eq 4.4.

$$\frac{C_e}{q_e} = \frac{1}{Q_0 b} + \frac{1}{Q_0} C_e$$

4.4)

q_e = the amount of metal adsorbed per gram of the adsorbent at equilibrium (mg/g), and C_e = the equilibrium concentration of adsorbate (mg L^{-1}). The maximum adsorption capacit can be calculated from slope of the linear equation form (Eq 4.4).
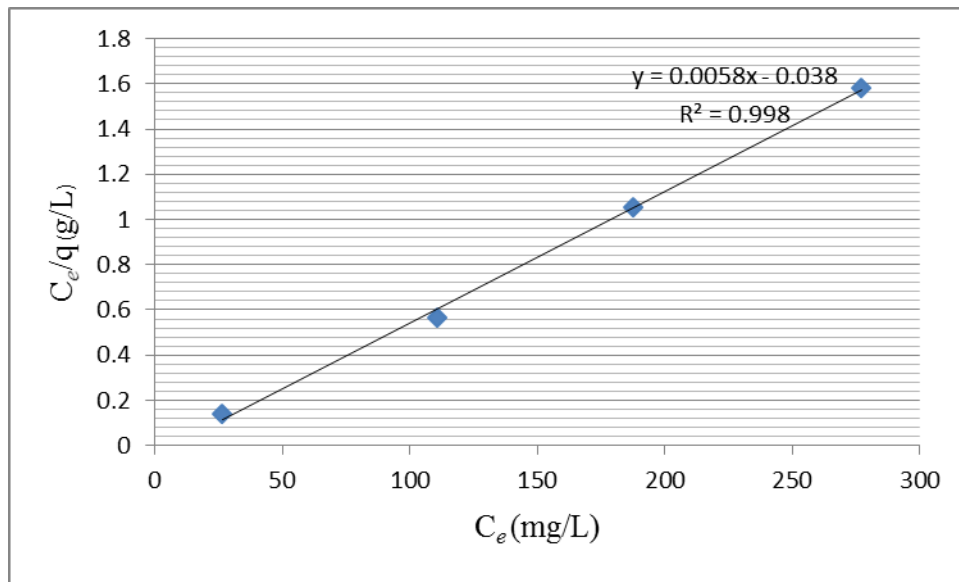
Figure 4.23 The Langmuir isotherm for Pb(II) sorption using DETA-MNPs@MCM-48.
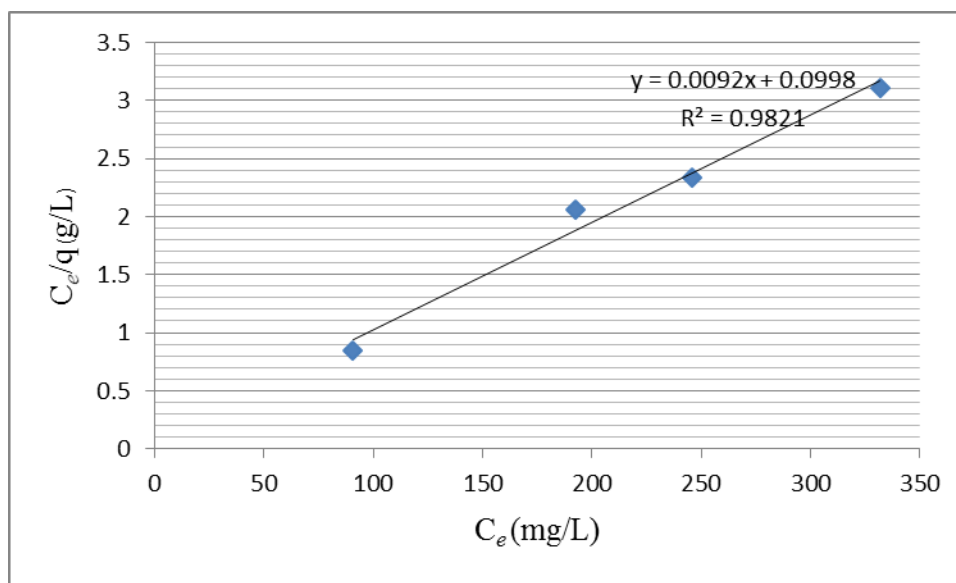
Figure 4.24 The Langmuir isotherm for Pb(II) sorption using AMTP-MNPs@MCM-48.

The Freundlich isotherm can be calculated with a linear form as shown in Eq. 4.5 as shown below

$$\ln q_e = \left(\frac{1}{n}\right)\ln C_e + \log k;$$

$$4.5)$$

where q_e = the amount of metal adsorbed per gram of the adsorbent at equilibrium (mg/g) and C_e = the equilibrium concentration of adsorbate (mg L^{-1}).
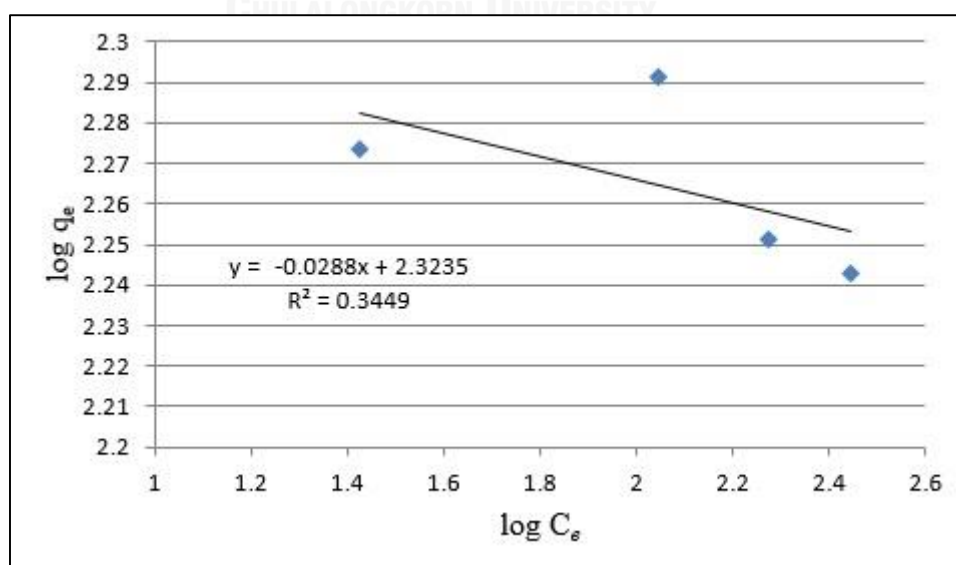
Figure 4.25 The Freundlich isotherm for Pb(II) sorption by DETA-MNPs@MCM-48.
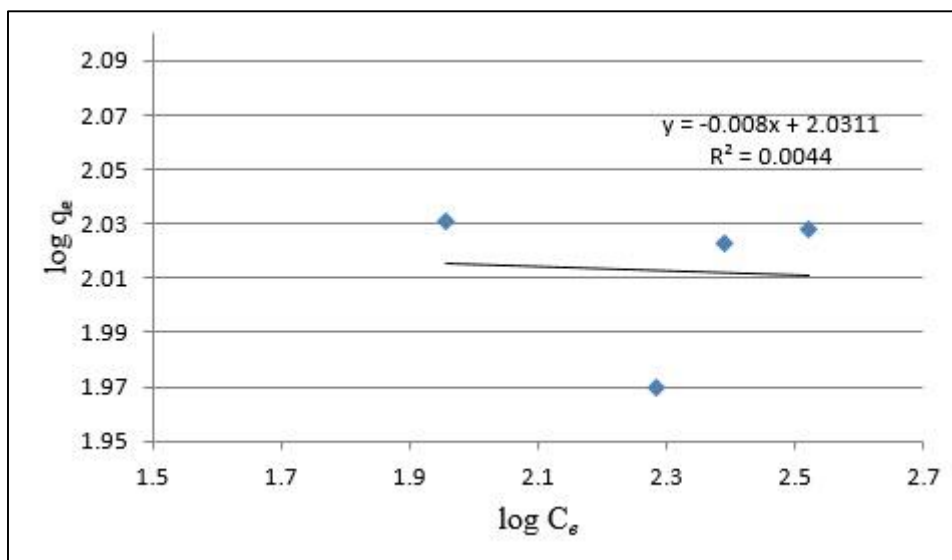
Figure 4.26 The Freundlich isotherm for Pb(II) sorption by AMTP-MNPs@MCM-48.

From the calculations, it could be implied that the Langmuir sorption model (Figure 4.24-4.25) matched better with the sorption behavior of the mesoporous adsorbents as the correlation coefficients value of the Langmuir isotherm of DETA-MNPs@MCM-48(R^2>0.99) and AMTP-MNPs@MCM-48 (R^2>0.98) are better than the Freundlich isotherm (Figure 4.26-4.27) of DETA-MNPs@MCM-48(R^2>0.3449) and AMTP-MNPs@MCM-48 (R^2>0.0044) .   Maximum capacities of Pb(II) sorption by DETA-MNPs@MCM-48 and AMTP-MNPs@MCM-48 were 172.43 mg/g and 108.69 mg/g, respectively, which is very close to the maximum adsorption capacities observed from the experiment on the effect of initial concentration of Pb (II) ion.

4.2.5. Effect of pH of Pb(II) ions solution

The experiments were conducted using 20 mg of DETA-MNPs@MCM-48 and AMTP-MNPs@MCM-48 added to 25 mL of lead solution of 100 mg/L. The experiments were performed at room temperature for 3 h. The pH of solution was varied at 1, 3, and 5. as shown in Figure 4.28 and Figure 4.29.
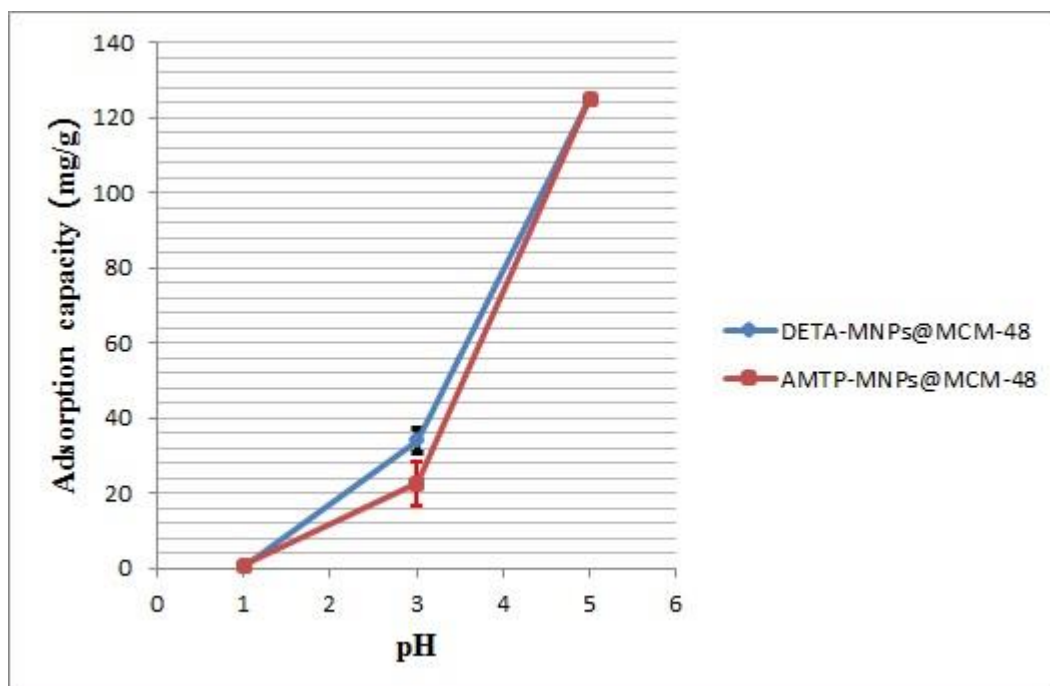
Figure 4 27 Effect of pH on lead adsorption capacity of DETA-MNPs@MCM-48 and AMTP-MNPs@MCM-48.
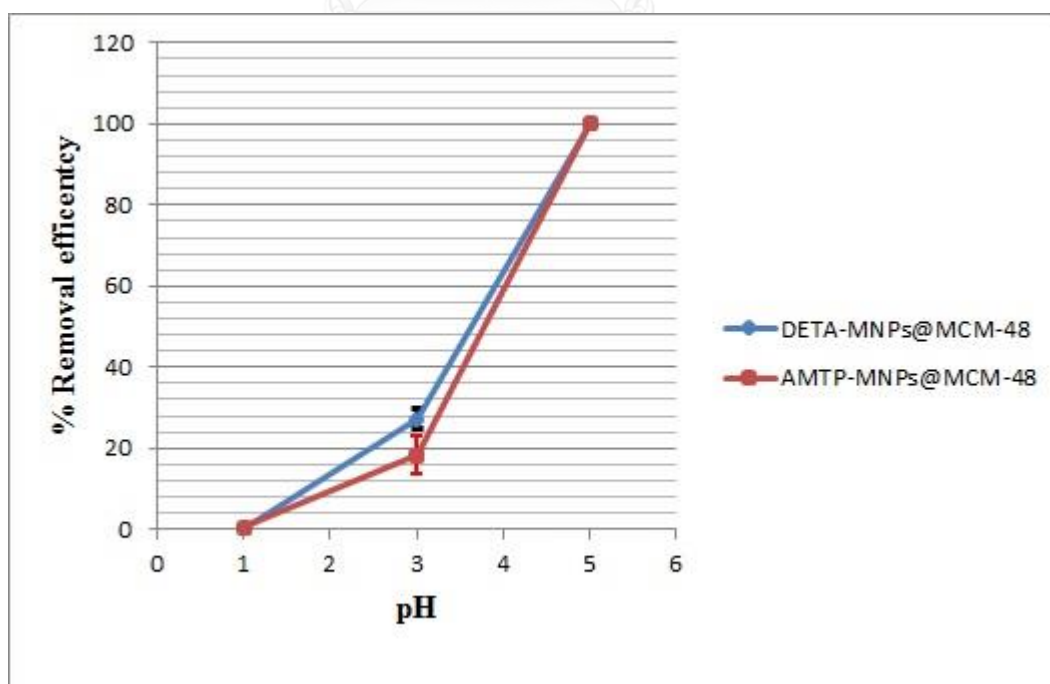
Figure 4.28 Effect of pH on lead ion removal efficiency of DETA-MNPs@MCM-48 and AMTP-MNPs@MCM-48.

The results indicated that the adsorption capacity and removal efficiency of DETA-MNPs@MCM-48 and AMTP-MNPs@MCM-48 increase with the increase of pH. At low pH, proton in acid solution can protonate binding sites of the chelating molecules. The surface of DETA-MNPs@MCM-48 and AMTP-MNPs@MCM-48 was covered by protonated form of the corresponding functional groups. In other words, the number of positively charged sites increased due to protonation in acidic environment. The decrease in adsorption efficiency and removal at lower pH may indicate that lead ions have to compete with proton to come in active sites of the sorbents. When solution became more basic, the corresponding functional groups on surface of DETA-MNPs@MCM-48 and AMTP-MNPs@MCM-48 were more deprotonated and became more negatively charged. Moreover, at higher pH, there were less competing proton for lead ions sorption on the active sites, the maximum capacity and the removal efficiency increased. For the lead solution with pH > 5, the sorption efficiency was decreased, and the accurate value cannot be determined with reliability due to the precipitation of $Pb(OH)_2$ at high pH [58]. The optimum for the highest adsorption of Pb(II) with DETA-MNPs @MCM-48 and AMTP-MNPs@MCM-48 were obtained at room temperature under pH 5 conditions where less protonation onto functional groups and no precipitation of the lead hydroxide, which could occur at high pH $(pH > 5)$.

4.2.6. Effect of contact time of Pb(II) ions solutions

The lead removal in 100 mg/L lead solution at different time intervals (15 to 240 min) on DETA-MNPs@MCM-48 and AMTP-MNPs@MCM-48. 20 mg of DETA-MNPs@MCM-48 and AMTP-MNPs@MCM-48 was added to lead solution at 30 °C with fixed pH at 5.
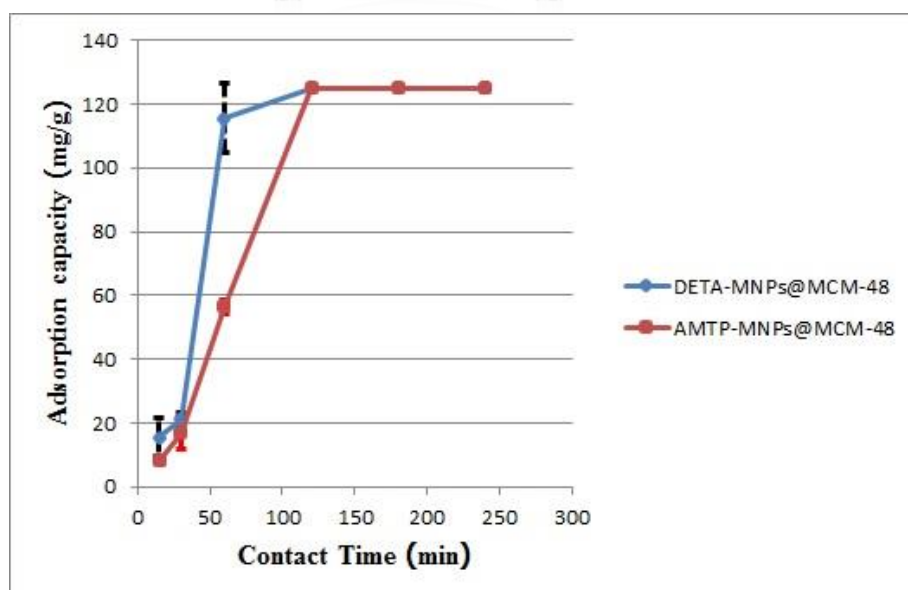
Figure 4.29 Effect of contact time on lead adsorption capacity of DETA-MNPs@MCM-48 and AMTP-MNPs@MCM-48.
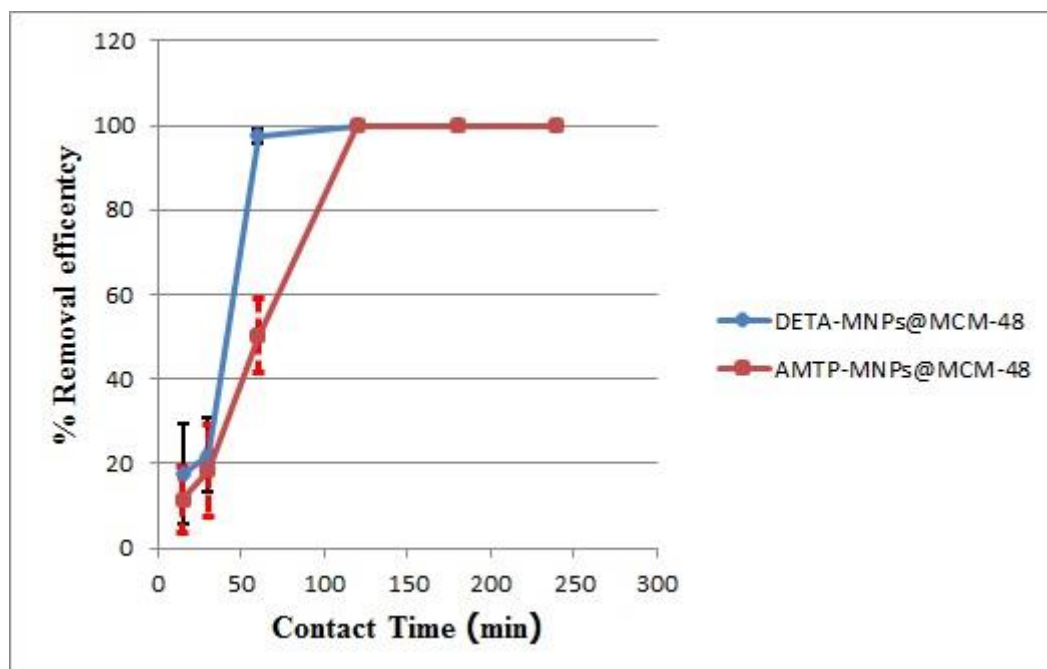
Figure 4.30 Effect of contact time on lead removal efficiency of DETA-
MNPs@MCM-48 and AMTP-MNPs@MCM-48.

For the effect of contact time （Figures 4.30-4.31） for the adsorption of lead
ion using DETA-MNPs@MCM-48 and AMTP-MNPs@MCM-48, the results showed
that the adsorption capacity and % removal efficiency increased with time until
reaching the equilibrium of lead adsorption within 2 h. The results indicated that in the
time ranging from 15 min to 2 h, DETA-MNPs@MCM-48 and AMTP-MNPs@MCM-
48 showed a good adsorption capacity and fast kinetics likely because at the starting
point the sorbents have a large number of active sites for metal-binding on the sorbent
surface. In other words, DETA-MNPs@MCM-48 and AMTP-MNPs@MCM-48 have
more adsorption appeared with more active sites available within 2 h. The equilibrium
was reached after 2 h indicating the saturation of active sites in sorbents.

4.2.7 Effect of foreign ions in Pb(II) removal operation

20 mg of DETA-MNPs@MCM-48 and AMTP-MNPs@MCM-48 was added
into 25 mL of mixture containing Pb^{2+} and one of the foreign ions, Zn^{2+}, Cd^{2+}, or Cr^{3+},
where the concentrations of each of metal ion are 100 mg/L with contact time 2 h as
shown in Figure 4.32.
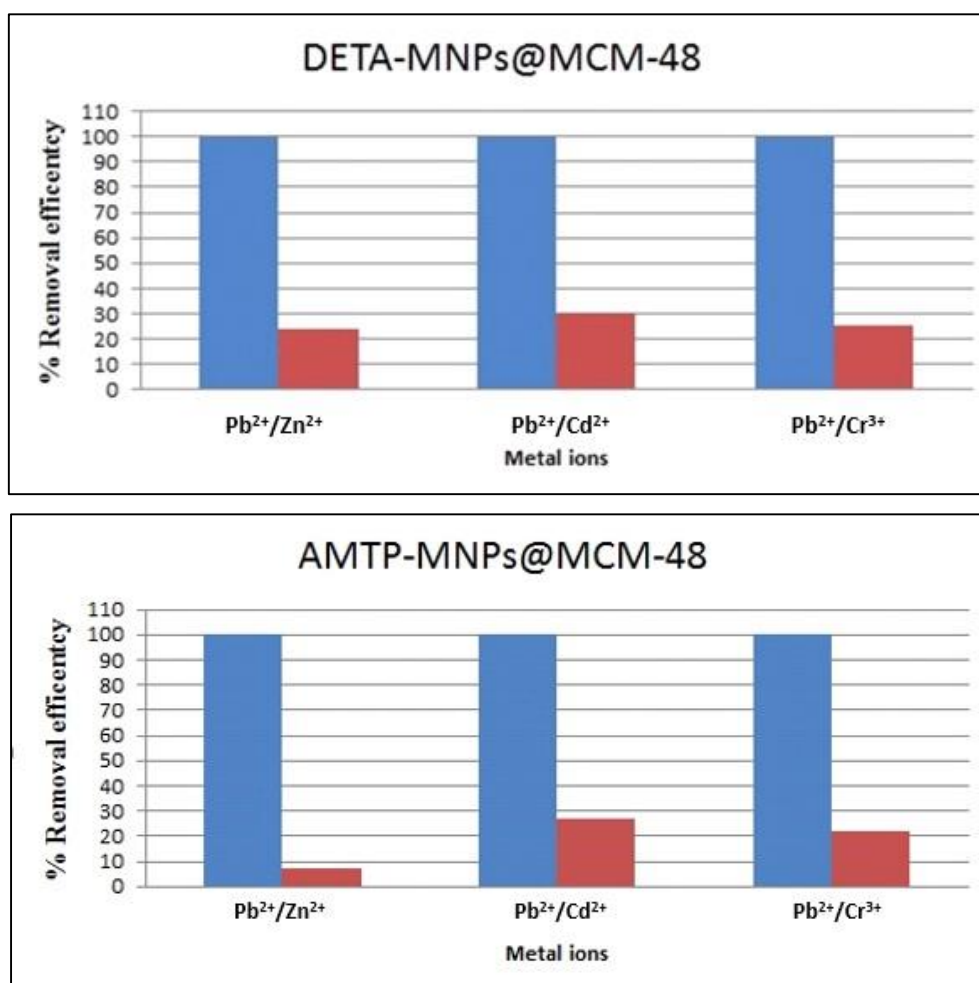
Figure 4.31 Selective adsorption of Pb(II) on DETA-MNPs@MCM-48 and AMTP-
MNPs@MCM-48. (sorbants = 20 mg, pH = 5, T = 30 °C, t = 120 min).

The results showed that the removal lead ions efficiency of DETA-
MNPs@MCM-48 and AMTP-MNPs@MCM-48 still have been found to be 100%
while DETA-MNPs@MCM-48 and AMTP-MNPs@MCM-48 could remove the other
metal ions less than 30%. It can be indicated that DETA-MNPs@MCM-48 and AMTP-
MNPs@MCM-48 exhibited good adsorption efficiency and selectivity to remove lead
in the mixture containing the other metal ions with a large quantity of competing metal
ions in the solution. The selectivity toward the adsorption of Pb^{2+} possibly because pore
sizes of both adsorbents and the active biding sites of the ligands inside the pore may
be specific to allow entrance of lead ion more than other metals in combination with
preference based on Hard-Soft Acid-Base theory.

4.2.8. Reusability of the DETA-MNPs@MCM-48 and AMTP-MNPs@MCM-48

20 mg of DETA-MNPs@MCM-48 and AMTP-MNPs@MCM-48 were
regenerated by washing with 10 mL of 1 M HCl and DI water for 1 h. The used sorbents

were dried at ambient temperature and was reused after regeneration as shown in Figure 4.33 and 4.44.
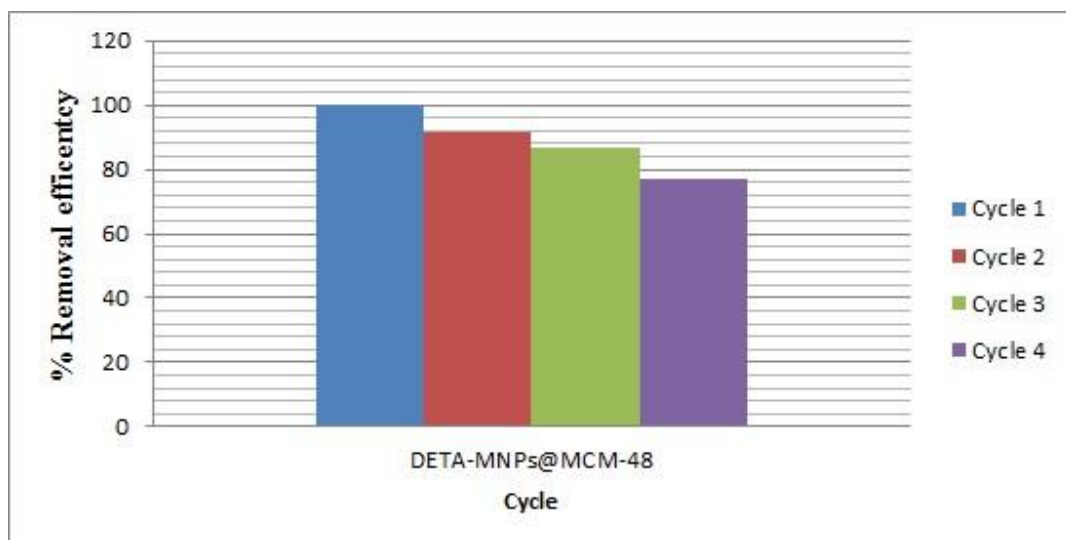
Figure 4.32 Reusability studies of the DETA-MNPs@MCM-48 adsorbent in several cycles.
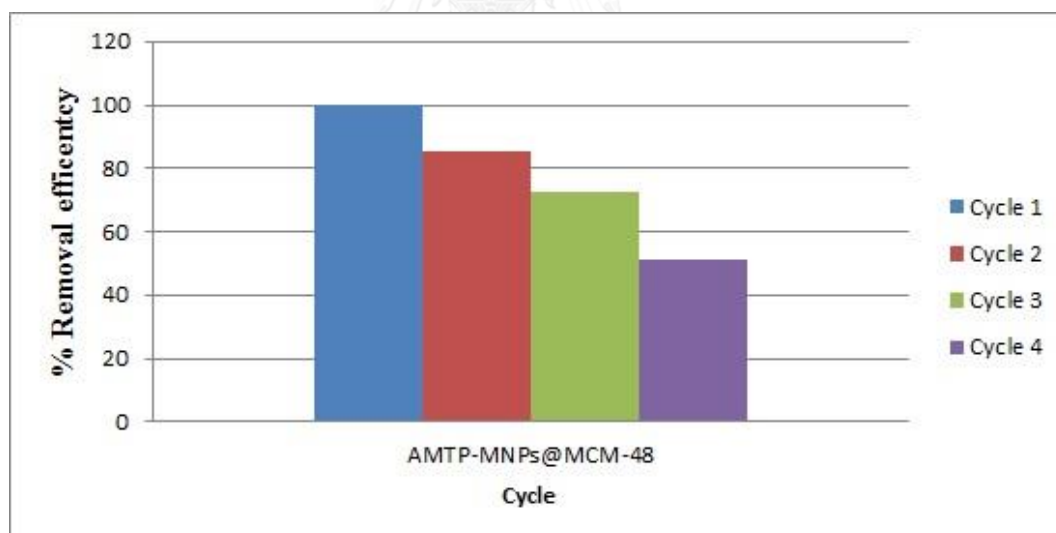
Figure 4.33 Reusability studies of the AMTP-MNPs@MCM-48 adsorbent in several cycles.

The results showed that the first and second cycles of DETA-MNPs@MCM-48 had a good performance of the sorbent, while more than 30% metal ion removal was achieved in the third cycles. For the fourth cycle of AMTP-MNPs@MCM-48, the removal efficiency went down to 51.13%. Therefore, the regeneration ability of heavy metal ion was not very effective using the current method because DETA-MNPs@MCM-48 and AMTP-MNPs@MCM-48 could not release lead ion from the functional groups on their surface when the DETA-MNPs@MCM-48 and AMTP-MNPs@MCM-48 were used in fourth and third cycles, respectively. The DETA-MNPs@MCM-48 and AMTP-MNPs@MCM-48 can be reused efficiently in that the sorbents could be used for at first cycles without significant change in the removal efficiency.

CHAPTER 5

CONCLUSION

MNPs@MCM-48 and MNPs@SBA-15 were prepared by combining mesoporous silicas and magnetic nanoparticles. The results from X-ray diffractometer (XRD), surface area analyzer, scanning electron microscope (SEM), and transmission electron microscope (TEM) confirmed that MNPs@MCM-48 and MNPs@SBA-15 composites were successfully prepared. MNPs@MCM-48 and MNPs@SBA-15 were modified with various ligands to improve lead adsorption efficiency. The functionalized-MNPs@MCM-48 and MNPs@SBA-15 were characterized using Fourier transforms infrared (FT-IR) spectrometer. In combination with FTIR, Ellman test and Ninhydrin test were used to confirm thiol group and amino group in the functionalized-MNPs@MCM-48 and MNPs@SBA-15. From the results, it was indicated that MNPs@MCM-48 and MNPs@SBA-15 composites were successfully modified.

From the results of lead adsorption from initial studies, DETA-MNPs@MCM-48 and ATP-MNPs@MCM-48 were chosen to be investigated in the removal of lead ions in aqueous solutions using batch operations. DETA-MNPs@MCM-48 and ATP-MNPs@MCM-48 were studied by thermogravimetric analysis (TGA) to confirm the thermal stability before adsorption test. The initial concentrations, adsorption isotherms, effect of contact time and effect of pH of lead solution were studied and the optimal conditions of using DETA-MNPs@MCM-48 and ATP-MNPs@ MCM-48 in adsorption of lead ions are showed in Table 5.1 and 5.2

Table 5.1 The adsorption behavior of DETA-MNPs@MCM-48 and optimal conditions for the removal of lead ions

Parameters	Adsorption behavior
Initial concentration to reach adsorption equilibrium	200 mg/L
Adsorption isotherm	Langmuir isotherm
Time to reach adsorption equilibrium	120 minutes
Solution pH	5
Maximum adsorption capacity (mg/g)	202.13 mg/g

Table 5.2 The adsorption behavior of ATP-MNPs@MCM-48 and and optimal conditions for the removal of lead ions

Parameters	Adsorption behavior
Initial concentration to reach adsorption equilibrium	100 mg/L
Adsorption isotherm	Langmuir isotherm
Time to reach adsorption equilibrium	120 minutes
Solution pH	5
Maximum adsorption capacity (mg/g)	125.00 mg/g

From the results, it was shown that the adsorption of lead ions onto DETA-MNPs@MCM-48 showed much higher efficiency in lead adsorption than ATP-MNPs@ MCM-48. The adsorption likely occurs mainly via coordination between $-NH_2$ and $-SH$ groups of the functionalized-MNPs@MCM-48 and lead ions in solutions and could be explained by HSAB theory and chelating effect.

DETA-MNPs@MCM-48 and ATP-MNPs@ MCM-48 showed a good lead removal efficiency in the mixture containing Pb^{2+} and either Cd^{2+}, Cr^{3+}, or Zn^{2+} ions, as the removal efficiency reach 100% in the conditions studied. The adsorbents could be regenerated using 1 M HCl as the eluent of lead ions in the used sorbents. The DETA-MNPs@MCM-48 and AMTP-MNPs@MCM-48 can be reused limitedly, as the sorbents could be used for in the second cycle with slight changes in the removal efficiency and adsorption capacity.

Suggestion of future work
- Various mesoporous silicas with the same ligands should be studied in more detail to find the best supporting materials for better performance in the adsorption applications.

- The number of reused cycle and the type of eluents should be investigated to improve the lead removal efficiency in the used sorbents.

REFERENCES

[1]   Cechinel, M.A.P., Ulson de Souza, S.M.A.G., and Ulson de Souza, A.A. Study of lead (II) adsorption onto activated carbon originating from cow bone. Journal of Cleaner Production 65 (2014): 342-349.

[2]   Wexler, P. Encyclopedia of Toxicology in Wexler, P. (ed.)Encyclopedia of Toxicology 3rd ed. England: Academic Press, 2004.

[3]   Grant, L.D. Lead and Compounds. in Environmental Toxicants, pp. 757-809: John Wiley & Sons, Inc., 2008.

[4]   Cleveland, L.M., Minter, M.L., Cobb, K.A., Scott, A.A., and German, V.F. Lead hazards for pregnant women and children: part 1: immigrants and the poor shoulder most of the burden of lead exposure in this country. Part 1 of a two-part article details how exposure happens, whom it affects, and the harm it can do. Am J Nurs 108(10) (2008): 40-9; quiz 50.

[5]   Ngueta, G., Prévost, M., Deshommes, E., Abdous, B., Gauvin, D., and Levallois, P. Exposure of young children to household water lead in the Montreal area (Canada): The potential influence of winter-to-summer changes in water lead levels on children's blood lead concentration. Environment International 73 (2014): 57-65.

[6]   Li, W., Zhang, L., Peng, J., Li, N., Zhang, S., and Guo, S. Tobacco stems as a low cost adsorbent for the removal of Pb(II) from wastewater: Equilibrium and kinetic studies. Industrial Crops and Products 28(3) (2008): 294-302.

[7]   Wang, H.J., Zhou, A.L., Peng, F., Yu, H., and Chen, L.F. Adsorption characteristic of acidified carbon nanotubes for heavy metal Pb(II) in aqueous solution. Materials Science and Engineering: A 466(1–2) (2007): 201-206.

[8]   Benhamou, A., Baudu, M., Derriche, Z., and Basly, J.P. Aqueous heavy metals removal on amine-functionalized Si-MCM-41 and Si-MCM-48. Journal of Hazardous Materials 171(1–3) (2009): 1001-1008.

[9]   Dolatyari, L., Yaftian, M.R., and Rostamnia, S. Removal of uranium(VI) ions from aqueous solutions using Schiff base functionalized SBA-15 mesoporous silica materials. Journal of Environmental Management 169 (2016): 8-17.

[10]   Zhang, M., et al. Preparation of core–shell magnetic ion-imprinted polymer for selective extraction of Pb(II) from environmental samples. Chemical Engineering Journal 178 (2011): 443-450.

[11]   Marlow, F. and Kleitz, F. Mesoporous silica fibers: internal structure and formation. Microporous and Mesoporous Materials 44–45 (2001): 671-677.

[12]   Eren, Z.S., Tunçer, S., Gezer, G., Yildirim, L.T., Banerjee, S., and Yilmaz, A. Improved solubility of celecoxib by inclusion in SBA-15 mesoporous silica: Drug loading in different solvents and release. Microporous and Mesoporous Materials 235 (2016): 211-223.

[13]   Øye, G., Sjöblom, J., and Stöcker, M. Synthesis and characterization of siliceous and aluminum-containing mesoporous materials from different surfactant solutions. Microporous and Mesoporous Materials 27(2–3) (1999): 171-180.

[14] Hoffmann, F., Cornelius, M., Morell, J., and Froba, M. Silica-based mesoporous organic-inorganic hybrid materials. Angew Chem Int Ed Engl 45(20) (2006): 3216-51.

[15] Elías, V.R., Oliva, M.I., Vaschetto, E.G., Urreta, S.E., Eimer, G.A., and Silvetti, S.P. Magnetic properties of iron loaded MCM-48 molecular sieves. Journal of Magnetism and Magnetic Materials 322(21) (2010): 3438-3442.

[16] Zhao, D., et al. Triblock copolymer syntheses of mesoporous silica with periodic 50 to 300 angstrom pores. Science 279(5350) (1998): 548-52.

[17] Cassiers, K., et al. A Detailed Study of Thermal, Hydrothermal, and Mechanical Stabilities of a Wide Range of Surfactant Assembled Mesoporous Silicas. Chemistry of Materials 14(5) (2002): 2317-2324.

[18] Hench, L.L. and West, J.K. The sol-gel process. Chemical Reviews 90(1) (1990): 33-72.

[19] Soler-Illia, G.J.d.A.A., Sanchez, C., Lebeau, B., and Patarin, J. Chemical Strategies To Design Textured Materials: from Microporous and Mesoporous Oxides to Nanonetworks and Hierarchical Structures. Chemical Reviews 102(11) (2002): 4093-4138.

[20] Beck, J.S., et al. A new family of mesoporous molecular sieves prepared with liquid crystal templates. Journal of the American Chemical Society 114(27) (1992): 10834-10843.

[21] Chen, C.-Y., Li, H.-X., and Davis, M.E. Studies on mesoporous materials. Microporous Materials 2(1) (1993): 17-26.

[22] Raman, N.K., Anderson, M.T., and Brinker, C.J. Template-Based Approaches to the Preparation of Amorphous, Nanoporous Silicas. Chemistry of Materials 8(8) (1996): 1682-1701.

[23] T. J. Keene, M., D. M. Gougeon, R., Denoyel, R., K. Harris, R., Rouquerol, J., and L. Llewellyn, P. Calcination of the MCM-41 mesophase: mechanism of surfactant thermal degradation and evolution of the porosity. Journal of Materials Chemistry 9(11) (1999): 2843-2849.

[24] Liu, Z., Terasaki, O., Ohsuna, T., Hiraga, K., Shin, H.J., and Ryoo, R. An HREM study of channel structures in mesoporous silica SBA-15 and platinum wires produced in the channels. Chemphyschem 2(4) (2001): 229-31.

[25] Buchel, G., Denoyel, R., Llewellyn, P.L., and Rouquerol, J. In situ surfactant removal from MCM-type mesostructures by ozone treatment. Journal of Materials Chemistry 11(2) (2001): 589-593.

[26] Zi, S.C., et al. New method to synthesize mesoporous titania by photodegradation of surfactant template. Solid State Sciences 52 (2016): 83-91.

[27] Huang, L., Kawi, S., Poh, C., Hidajat, K., and Ng, S.C. Extraction of cationic surfactant templates from mesoporous materials by CH_3OH-modified CO_2 supercritical fluid. Talanta 66(4) (2005): 943-951.

[28] Wu, W., Wu, Z., Yu, T., Jiang, C., and Kim, W.-S. Recent progress on magnetic iron oxide nanoparticles: synthesis, surface functional strategies and biomedical applications. Science and Technology of Advanced Materials 16(2) (2015): 023501.

[29] Bedanta, S., Petracic, O., and Kleemann, W. . Chapter 1 - Supermagnetism. in K.H.J (ed.)Handbook of Magnetic Materials, 2015.

[30]   Coey, J.M.D. <u>Magnetism and Magnetic materials</u>. Cambridge University Press, 2010.

[31]   Blaney, L. Magnetite (Fe_3O_4): Properties, Synthesis, and Applications. <u>The Lehigh review</u> (2007).

[32]   Jones, M.M. and Vaughn, W.K. HSAB theory and acute metal ion toxicity and detoxification processes. <u>Journal of Inorganic and Nuclear Chemistry</u> 40(12) (1978): 2081-2088.

[33]   Inbaraj, B.S. and Chen, B.-H. In vitro removal of toxic heavy metals by poly(γ-glutamic acid)-coated superparamagnetic nanoparticles. <u>International Journal of Nanomedicine</u> 7 (2012): 4419-4432.

[34]   Baytak, S. and Arslan, Z. Solid Phase Extraction of Trace Elements in Waterand Tissue Samples on a Mini Column with Diphenylcarbazone Impregnated Nano-TiO(2) and Their Determination by Inductively Coupled Plasma Optical Emission Spectrometry. <u>Clean : soil, air, water</u> 43(6) (2015): 822-829.

[35]   Jang, A., Seo, Y., and Bishop, P.L. The removal of heavy metals in urban runoff by sorption on mulch. <u>Environmental Pollution</u> 133(1) (2005): 117-127.

[36]   Saliba, R., Gauthier, H., Gauthier, R., and Petit-Ramel, M. Adsorption of copper(II) and chromium(III) ions onto amidoximated cellulose. <u>Journal of Applied Polymer Science</u> 75(13) (2000): 1624-1631.

[37]   Yang, H., Xu, R., Xue, X., Li, F., and Li, G. Hybrid surfactant-templated mesoporous silica formed in ethanol and its application for heavy metal removal. <u>Journal of Hazardous Materials</u> 152(2) (2008): 690-698.

[38]   Thu, P.T.T., Thanh, T.T., Phi, H.N., Kim, S.J., and Vo, V. Adsorption of lead from water by thiol-functionalized SBA-15 silicas. <u>Journal of Materials Science</u> 45(11) (2010): 2952-2957.

[39]   Idris, S.A., Davidson, C.M., McManamon, C., Morris, M.A., Anderson, P., and Gibson, L.T. Large pore diameter MCM-41 and its application for lead removal from aqueous media. <u>Journal of Hazardous Materials</u> 185(2–3) (2011): 898-904.

[40]   Mehdinia, A., Shegefti, S., and Shemirani, F. Removal of Lead(II), Copper(II) and Zinc(II) Ions from Aqueous Solutions Using Magnetic Amine-Functionalized Mesoporous Silica Nanocomposites. <u>Journal of the Brazilian Chemical Society</u> 26 (2015): 2249-2257.

[41]   Anbia, M., Kargosha, K., and Khoshbooei, S. Heavy metal ions removal from aqueous media by modified magnetic mesoporous silica MCM-48. <u>Chemical Engineering Research and Design</u> 93 (2015): 779-788.

[42]   Gies, H., et al. Synthesis and characterization of silica MCM-48 as carrier of size-confined nanocrystalline metal oxides particles inside the pore system. <u>Microporous and Mesoporous Materials</u> 60(1–3) (2003): 31-42.

[43]   Zhao, D., Huo, Q., Feng, J., Chmelka, B.F., and Stucky, G.D. Nonionic Triblock and Star Diblock Copolymer and Oligomeric Surfactant Syntheses of Highly Ordered, Hydrothermally Stable, Mesoporous Silica Structures. <u>Journal of the American Chemical Society</u> 120(24) (1998): 6024-6036.

[44]   Park, J., et al. Ultra-large-scale syntheses of monodisperse nanocrystals. <u>Nat Mater</u> 3(12) (2004): 891-895.

[45]   Test methods for evaluating solid waste : physical/chemical methods (SW-846). 1996, Version 1. Washington, D.C. : U.S. Environmental Protection Agency, Office of Solid Waste ; Springfield, Va. : U.S. Dept. of Commerce, National Technical Information Service, 1996.

[46]   Bibby, A. and Mercier, L. Mercury(II) Ion Adsorption Behavior in Thiol-Functionalized Mesoporous Silica Microspheres. Chemistry of Materials 14(4) (2002): 1591-1597.

[47]   Olkhovyk, O., Antochshuk, V., and Jaroniec, M. Benzoylthiourea-modified MCM-48 mesoporous silica for mercury(II) adsorption from aqueous solutions. Colloids and Surfaces A: Physicochemical and Engineering Aspects 236(1–3) (2004): 69-72.

[48]   Zhang, L., Shao, H.-p., Zheng, H., Lin, T., and Guo, Z.-m. Synthesis and characterization of $Fe_3O_4@SiO_2$ magnetic composite nanoparticles by a one-pot process. International Journal of Minerals, Metallurgy, and Materials 23(9) (2016): 1112-1118.

[49]   Pérez-Quintanilla, D., Sánchez, A., del Hierro, I., Fajardo, M., and Sierra, I. Preparation, characterization, and Zn2+ adsorption behavior of chemically modified MCM-41 with 5-mercapto-1-methyltetrazole. Journal of Colloid and Interface Science 313(2) (2007): 551-562.

[50]   Li, Y.S., Wang, Y., Tran, T., and Perkins, A. Vibrational spectroscopic studies of (3-mercaptopropyl)trimethoxylsilane sol-gel and its coating. Spectrochim Acta A Mol Biomol Spectrosc 61(13-14) (2005): 3032-7.

[51]   Costa, J.A.S., Garcia, A.C.F.S., Santos, D.O., Sarmento, V.H.V., de Mesquita, M.E., and Romão, L.P.C. Applications of inorganic–organic mesoporous materials constructed by self-assembly processes for removal of benzo[k]fluoranthene and benzo[b]fluoranthene. Journal of Sol-Gel Science and Technology 75(3) (2015): 495-507.

[52]   Loganathan, S. and Ghoshal, A.K. Amine tethered pore-expanded MCM-41: A promising adsorbent for CO_2 capture. Chemical Engineering Journal 308 (2017): 827-839.

[53]   Sun, X.-Y., Li, P.-Z., Ai, B., and Wang, Y.-B. Surface modification of MCM-41 and its application in DNA adsorption. Chinese Chemical Letters 27(1) (2016): 139-144.

[54]   Nale, D.B., Rana, S., Parida, K., and Bhanage, B.M. Amine functionalized MCM-41 as a green, efficient, and heterogeneous catalyst for the regioselective synthesis of 5-aryl-2-oxazolidinones, from CO2 and aziridines. Applied Catalysis A: General 469 (2014): 340-349.

[55]   Das, S. and Dhar, B.B. Green synthesis of noble metal nanoparticles using cysteine-modified silk fibroin: catalysis and antibacterial activity. RSC Advances 4(86) (2014): 46285-46292.

[56]   Chen, F., Hong, M., You, W., Li, C., and Yu, Y. Simultaneous efficient adsorption of Pb2+ and MnO4− ions by MCM-41 functionalized with amine and nitrilotriacetic acid anhydride. Applied Surface Science 357, Part A (2015): 856-865.

[57]   Kumar, S.V., Huang, N.M., Lim, H.N., Zainy, M., Harrison, I., and Chia, C.H. Preparation of highly water dispersible functional graphene/silver

nanocomposite for the detection of melamine. <u>Sensors and Actuators B: Chemical</u> 181 (2013): 885-893.

[58]   Ebrahimzadeh, H., Asgharinezhad, A.A., Moazzen, E., Amini, M.M., and Sadeghi, O. A magnetic ion-imprinted polymer for lead(II) determination: A study on the adsorption of lead(II) by beverages. <u>Journal of Food Composition and Analysis</u> 41 (2015): 74-80.

APPENDIX

VITA

Mr. Chawalit Takoon was born on November 6, 1988 in Bangkok,Thailand. In 2012, he graduated in Bachelor's Degree of Science in Chemistry from Srinakarinwirot University. In next two years, he began his Master of Science in the program of Petrochemistry and Polymer Science at Chulalongkorn University and completed in 2016.

He presented "Modifications of MCM-48 Mesoporous Silica for Lead(Il) Removal and the Formation of its Nanocomposites with Iron Oxide Nanoparticles" in Pure and Applied Chemistry International Conference (PACCON 2016) at BITEC by poster presentation.

His present address is 25/6 Thanon Phutthamonthon Sai 1, Bang Ramat, Taling Chan, Bangkok, 10170, E-mail address : topo-006@hotmail.com Mobile: 087-715-7331

จุฬาลงกรณ์มหาวิทยาลัย
CHULALONGKORN UNIVERSITY